CO$_2$ HYDROGENATION TO METHANOL OVER SUPPORTED COPPER AND GALLIUM BASED CATALYSTS AT THE ATMOSPHERIC PRESSURE

A THESIS SUBMITTED TO
THE GRADUATE SCHOOL OF NATURAL AND APPLIED SCIENCES
OF
MIDDLE EAST TECHNICAL UNIVERSITY

BY

SEZER OSMANAĞA

IN PARTIAL FULFILLMENT OF THE REQUIREMENTS
FOR
THE DEGREE OF MASTER OF SCIENCE
IN
CHEMICAL ENGINEERING

AUGUST 2022

Approval of the thesis:

CO$_2$ HYDROGENATION TO METHANOL OVER SUPPORTED COPPER AND GALLIUM BASED CATALYSTS AT THE ATMOSPHERIC PRESSURE

submitted by **SEZER OSMANAĞA** in partial fulfillment of the requirements for the degree of **Master of Science** in **Chemical Engineering, Middle East Technical University** by,

Prof. Dr. Halil Kalıpçılar
Dean, Graduate School of **Natural and Applied Sciences** _____

Prof. Dr. Pınar Çalık
Head of the Department, **Chemical Engineering** _____

Assoc. Prof. Dr. Bahar İpek Torun
Supervisor, **Chemical Engineering, METU** _____

Prof. Dr. Işık Önal
Co-Supervisor, **Chemical Engineering, METU** _____

Examining Committee Members:

Prof. Dr. Deniz Üner
Chemical Engineering, METU _____

Prof. Dr. Işık Önal
Chemical Engineering, METU _____

Assoc. Prof. Dr. Bahar İpek Torun
Chemical Engineering, METU _____

Asst. Prof. Dr. Gökhan Çelik
Chemical Engineering, METU _____

Asst. Prof. Dr. Murat Oluş Özbek
Chemical Engineering, GTU _____

Date: 08.08.2022

I hereby declare that all information in this document has been obtained and presented in accordance with academic rules and ethical conduct. I also declare that, as required by these rules and conduct, I have fully cited and referenced all material and results that are not original to this work.

Name Last name : Sezer Osmanağa

Signature :

ABSTRACT

CO₂ HYDROGENATION TO METHANOL OVER SUPPORTED COPPER AND GALLIUM BASED CATALYSTS AT THE ATMOSPHERIC PRESSURE

Osmanağa, Sezer
Master of Science, Chemical Engineering
Supervisor: Assoc. Prof. Dr. Bahar İpek Torun
Co-Supervisor: Prof. Dr. Işık Önal

August 2022, 69 pages

The continuous increase of the CO_2 concentration in the atmosphere has been negatively impacting the environment, due to its contribution in the global warming. Hence, it is necessary for the current CO_2 valorization techniques to advance in order to make use of CO_2. A possible technique is the CO_2 hydrogenation to methanol and DME. The process of CO_2 hydrogenation to methanol has been taking place in industry for about a century. However, due to the thermodynamic limitation imposed by the reaction stoichiometry, it has been carried out at elevated pressures of about 50−100 bar to achieve high yield. Due to the high cost of supplying high pressure, it is desired to run the process at low pressures. Furthermore, it is known that dehydrating methanol into dimethyl ether (DME) via a solid acid catalyst improves the methanol and DME selectivity by suppressing the formation of the side product, CO. Catalysts that can achieve both methanol and DME production are bifunctional catalyst such as Cu catalysts supported on solid acid catalysts, such as zeolites or γ-Al_2O_3.

In this study, the CO_2 hydrogenation to methanol is carried out at atmospheric pressure, using Cu based catalysts. Different supports, including γ-Al_2O_3, H^+-ZSM5, and CeO_2, and different promoters, including Ga, Ho and La are used to prepare different catalysts with different promoter concentrations. Results showed that Cu containing and 5 wt. % Ga promoted γ-Al_2O_3 catalyst (10Cu-5Ga/γ-Al_2O_3) had the highest combined methanol and DME activity and selectivity, showing methanol and DME formation rates of 52.5 and 96.5 μmol g_{cat}^{-1} h^{-1}, respectively, and a combined selectivity of 20.5%. Those results were recorded at the optimized reaction conditions, at a temperature of 220 °C, feed ratio of $9H_2/1CO_2$, and gas hourly space velocity (GHSV) of 25,000 h^{-1}.

ÖZ

ATMOSFERİK BASINÇTA DESTEKLİ BAKIR VE GALYUM İÇEREN KATALİZÖRLERLE KARBONDİOKSİT HİDROJENLENMESİ İLE METANOL ELDESİ

Osmanağa, Sezer
Yüksek Lisans, Kimya Mühendisliği
Tez Yöneticisi: Doç. Dr. Bahar İpek Torun
Ortak Tez Yöneticisi: Prof. Dr. Işık Önal

Ağustos 2022, 69 sayfa

Atmosferdeki CO_2 konsantrasyonunun sürekli artması, küresel ısınmaya etkisi nedeniyle çevreyi olumsuz etkilemektedir. Bu nedenle, CO_2'den yararlanmak için mevcut CO_2 değerleme tekniklerinin ilerletilmesi gerekmektedir. Olası bir teknik, CO_2'nin metanol ve DME'e hidrojenasyonudur. CO_2'nin metanole hidrojenlenmesi yaklaşık bir asırdır endüstride kullanılmaktadır. Fakat, reaksiyon stokiyometrisinin getirdiği termodinamik kısıtlama nedeniyle, yüksek verim elde etmek için yaklaşık 50-100 bar'lık yüksek basınçlarda çalışılmaktadır. Yüksek basınç sağlamanın yüksek maliyeti nedeniyle işlemin düşük basınçlarda çalıştırılması istenmektedir. Ayrıca, bir katı asit katalizörü aracılığıyla metanolün dimetil etere (DME) dehidre edilmesinin, yan ürün CO oluşumunu baskılayarak methanol ve DME seçiciliğini iyileştirdiği bilinmektedir. Hem metanol hem de DME üretimini gerçekleştirebilen katalizörler, zeolitler veya γ-Al_2O_3 gibi katı asit katalizörleri üzerinde desteklenen Cu katalizörleri gibi, iki işlevli katalizörlerdir.

Bu çalışmada, CO_2'nin metanole hidrojenasyonu, Cu bazlı katalizörler kullanılarak atmosfer basıncında gerçekleştirilmiştir. Katalizör olarak farklı konsantrasyonlara

sahip Ga, Ho ve La dahil olmak üzere farklı promotörler, γ-Al_2O_3, H^+-ZSM5 ve CeO_2 dahil olmak üzere farklı destekler üzerinde kullanılmıştır. Sonuçlar, Cu içeren ve ağırlıkça %5 Ga ile desteklenen γ-Al_2O_3 katalizörünün (10Cu-5Ga/γ-Al_2O_3) en yüksek kombine metanol ve DME aktivitesine, sırasıyla 52,5 ve 96,5 μmol g_{cat}^{-1} h^{-1} oluşum hızları, ve toplam %20,5 seçiciliğe sahip olduğunu göstermiştir. Bu sonuçlar, optimize edilmiş reaksiyon koşullarında: 220 °C sıcaklıkta, 9H_2/1CO_2 besleme oranında ve 25.000 h^{-1} gaz saatlik boşluk hızında (GHSV) elde edilmiştir.

Anahtar Kelimeler: Kataliz, CO_2 Hidrojenasyonu, Metanol, Atmosferik Basınç

To my mother and father

need an eternity to pay back, and my father who has no bigger dream than seeing me successful and achieve my goals.

TABLE OF CONTENTS

LIST OF TABLES

LIST OF FIGURES

FIGURES

LIST OF ABBREVIATIONS

ABBREVIATIONS

MeOH	Methanol
DME	Dimethyl Ether
XRD	X-Ray Diffraction
TEM	Transmission Electron Microscopy
ICP-OES	Inductively Coupled Plasma-Optical Emission Spectroscopy
TPR	Temperature Programmed Reduction

LIST OF SYMBOLS

SYMBOLS

T   Temperature, °C

P   Pressure, bar

v   Volumetric Flowrate, cm^3/min

λ   Wavelength, Å

D   Dispersion, %

d_c Crystal Size, nm

d_p Particle Size, nm

X   Conversion, %

S   Selectivity, %

r   Rate, $\mu mol\ g_{cat}^{-1}\ h^{-1}$

CHAPTER 1

INTRODUCTION

The continuous industrial development has been coupled with the rise of CO_2 emissions to the atmosphere, resulting in an ascending pattern of the CO_2 concentration levels, keeping it currently the second most abundant greenhouse gas in the atmosphere (after water vapor) with a concentration of 421 ppm as of May 2022[1]. The increase of the concentration of CO_2 has been correlated to climate change phenomena, mainly due to its effect in increasing the temperature of the atmosphere. The increase in the temperature causes melting of the ice sheets and shelves, resulting in an increase in the sea level, as well as an increase in the water vapor in the atmosphere, causing the temperature to increase even more, exhibiting a positive feedback loop. As per the aforementioned negative effects of CO_2 abundance in the atmosphere, it is necessary to valorize it. There are various straightforward pathways to use CO_2, such as using it in fire extinguishers, in carbonated beverages, and as a working fluid for electricity[2]. However, such applications are not enough to make a difference in CO_2 concentration in the atmosphere[3]. Hence, the application of chemical valorization techniques of CO_2 into other valuable chemicals is necessary[4].

1.1 CO_2 Valorization via Chemical Routes

There are various chemical reactions that can valorize CO_2 into valuable chemicals. In this section, those techniques will be explained briefly.

1.1.1 CO₂ Hydrogenation to Methanol and Dimethyl Ether

Methanol is used as a feedstock for the production of multiple other derivatives, such as dimethyl ether(5) and olefins(6). Dimethyl ether can be used in diesel engines, which, like methanol, also emits minimal soot(7) and is also biodegradable(8). Both methanol and DME are easy to transport, considering methanol is liquid under ambient temperature and pressure(9), and DME is liquid at a relatively low pressure, similar to liquified petroleum gas(10). Since of the beginning of the industrial synthesis of methanol production in 1923 from syngas, the process was taking place at pressures above 300 bar, and temperatures of 300–400 °C over Cr_2O_3-ZnO catalysts(11). A few decades later, the process of methanol production from syngas (H_2+CO_2+CO) has been carried out in industry at temperatures of about 220–250 °C and elevated pressures of about 50–100 bar(12) over $Cu/ZnO/Al_2O_3$, upon its invention in 1947(11). As for DME, one common way of producing it is from methanol dehydration reaction using solid acid catalysts, or indirectly from CO_2, after producing methanol(5).

1.1.2 CO₂ Conversion to Methane, Syngas and Olefins

CO_2 can be valorized via methanation, also named Sabatier reaction (see Eq. 1.1), which is achieved by hydrogenating CO_2 at elevated temperatures and pressures of about 500 °C and 30 bar, respectively, to produce methane(5,6). In addition, CO_2 can be used as a reactant in both steam reforming (SR) and dry methane reforming (DMR) to produce syngas(4). It is possible to combine both of the processes, SR (Eq. 1.2, 1.3) and DMR (Eq. 1.4) to emit less CO_2 compared to DMR alone, as the CO_2 can be used back to form syngas via SR(15). Furthermore, CO_2 can be converted into lighter olefins, such as ethylene and propylene, which are highly produced (16) and demanded as feedstocks for the production of polymers(17). This valorization technique can be achieved either via CO_2 hydrogenation to methanol first, then

converting methanol to olefins, or via direct hydrogenation of CO_2 to olefins, at temperatures of 350–400 °C and pressures of around 30 bar (6)(18).

$$CO_2 + 4H_2 \rightleftharpoons CH_4 + 2H_2O \qquad \Delta H^o = -164.9 \frac{kJ}{mol} \qquad \text{Eq. 1.1}$$

$$CH_4 + H_2O \rightleftharpoons CO + H_2 \qquad \Delta H^o = +206.1 \frac{kJ}{mol} \qquad \text{Eq. 1.2}$$

$$CO_2 + H_2 \rightleftharpoons CO + H_2O \qquad \Delta H^o = +41.2 \frac{kJ}{mol} \qquad \text{Eq. 1.3}$$

$$CO_2 + CH_4 \rightleftharpoons 2CO + 2H_2 \qquad \Delta H^o = +247.3 \frac{kJ}{mol} \qquad \text{Eq. 1.4}$$
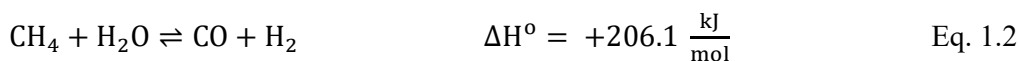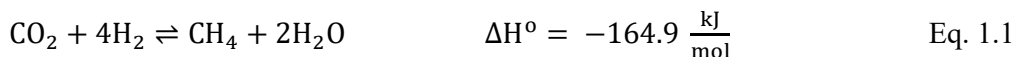
1.2   Thermodynamic Analysis of CO_2 Hydrogenation to Methanol and DME

CO_2 hydrogenation to methanol is carried out industrially, as mentioned previously, at elevated pressures of 50–100 bar(12). As can be seen from the stoichiometry of reaction (Eq. 1.5); higher pressure is favored for higher conversion of CO_2 to methanol. The challenge, however, is not only the conversion, but also the selectivity of the reaction, as the parallel reaction (Eq. 1.3) known as the reverse water gas shift reaction (rWGS) produces CO as an undesired byproduct, decreasing the selectivity of methanol.

$$CO_2 + 3\,H_2 \rightleftharpoons CH_3OH + H_2O \qquad \Delta H^o = -49.5 \text{ kJ/mol} \qquad \text{Eq. 1.5}$$

$$CO_2 + H_2 \rightleftharpoons CO + H_2O \qquad \Delta H^o = +41.2 \text{ kJ/mol} \qquad \text{Eq. 1.3}$$

As can be seen from the stoichiometry of the reaction, the rWGS reaction is favored at low pressures, as opposed to CO_2 hydrogenation to methanol. In order to shift equilibrium away from CO, taking methanol dehydration to DME reaction into account is necessary. The dehydration reaction of methanol to DME, represented by the reaction equation (Eq. 1.6), has a stoichiometry that helps the reaction to be favored at low pressures.

$$2\ CH_3OH \rightleftharpoons CH_3OCH_3 + H_2O \qquad \Delta H^o = -23.0\ kJ/mol \qquad \text{Eq. 1.6}$$

This way, if part of the formed methanol is dehydrated into DME, it is possible to produce more and have a higher selectivity of methanol and DME, as can be seen in Fig. 1.1(19). The pressure at which the reaction takes place, however, is not the only critical parameter. Looking at the enthalpy of the reactions, the temperature is necessary to be low in order to have a higher selectivity of methanol, as both of the favored reactions are exothermic reaction, while rWGS is endothermic. The challenge, however, is that even if methanol and DME are produced with high selectivity, in order to have a high conversion, and hence a high yield, high enough temperatures are required to activate the reaction kinetically. The balance between high selectivity and yield requires the use of catalysts to selectively activate a reaction (CO_2 to methanol) over the other (rWGS).
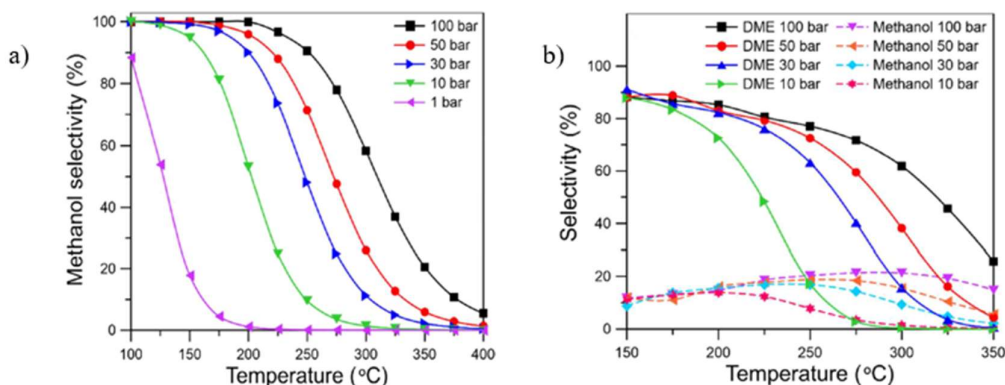
Figure 1.1 Thermodynamic conversion of CO_2 and selectivity of a) methanol and b) methanol and DME at different temperatures pressures(19)

1.3   Cu Based Catalysts

Considering that there are extensive studies on CO_2 hydrogenation to methanol, there are many catalysts in literature that were synthesized and tested. As a catalyst for methanol synthesis, Cu has been the most investigated catalyst. However, activity exhibited by Cu alone is not enough to allow it to be used for large scale production(20). In order to enhance it, supports and promoters have been

incorporated with Cu to enhance the activity and selectivity(21), not only for methanol production, but also for DME production(22). The most commonly used catalyst in the industry for CO_2 hydrogenation to methanol is $Cu/ZnO/Al_2O_3$(23), in which ZnO and Al_2O_3 act as promoters. In this section, Cu based catalysts are investigated, in terms of structure sensitivity and particle size, promoters and supports.

1.3.1 Structure Sensitivity and Particle Size

The relationship between copper particle size and production and selectivity of methanol has been studied on different catalysts in literature, and the exact relation is debatable. A study on $Cu-ZnO/ZrO_2$ for Cu particle sizes in the range 2−32 nm, showed that the turnover frequency (TOF) increases proportionally with Cu particle size, as small particles may be able to more strongly adsorb intermediate species, such as water and formate(24). Another study on Cu/ZnO for particle sizes in the range 8.5−37.3 nm showed no effect resulted from the change in Cu particle size(25). On the other hand, a study on Cu/Zr, Cu/Zn/Zr, and Cu/Zn/Zr/Ga/Y, with particle sizes of 27, 16, and 6 nm, respectively, showed a higher formation rate for Cu/Zn/Zr/Ga/Y, attributing that to the small Cu particles having a larger number of step and edge sites, which are more reactive than coordinated sites(26).

The previous studies were conducted over supported and promoted Cu where metal-support and promoter interactions are strong. Barberis et al. (27) studied the intrinsic effect of particle size on Cu, where Cu is supported on graphitic carbon, which is a relatively inert support and does not interact strongly with Cu. The study was conducted on particles of sizes between 3 and 30 nm. The results showed that smaller particles exhibited better selectivity towards methanol, where higher formate coverage was found, along with higher fraction of less coordinated sites (e.g., corners and edges). As the particle size increased, formate coverage, less coordinated sites, and methanol selectivity decreased.

1.3.2 Catalyst Promoters

1.3.2.1 Zinc

As mentioned earlier, the most commonly used catalyst in the industry is the commercial catalyst $Cu/ZnO/Al_2O_3$(23). There are extensive studies on the promotional effect observed upon the addition of zinc, attributing the activity to the strong metal support interaction (SMSI)(28). A study by Behren et al was able to illustrate the SMSI effect between Cu and ZnO(29). After reduction, it was observed that close to the steps, the Cu:Zn ratio is inverted from 70:30 for the calcined catalyst, to 30:70 upon reduction, forming CuZn alloy. During the reaction, zinc exists in a partially oxidized state $Zn^{\delta+}$ due to the reduction by SMSI, and oxidation upon the adsorption of intermediates such as formate and hydroxyl. The partial substitution of Cu by Zn results in an increase in the binding strength of the intermediates, resulting in higher activity upon the addition of zinc.

1.3.2.2 Gallium

Gallium has been used in multiple studies as a promoter for Cu based catalysts(26,30–33).According to a study by Medina et al(34) on SiO_2 supported Cu catalyst, the addition of Ga was found to increase the dispersion of Cu using XPS as the Ga content increases from 1 to 5 %, while the dispersion drops when 10% is used. Similar effect was found from another XPS study(26), where the addition of Ga to $Cu/ZnO/ZrO_2$ resulted in a higher fraction of Cu on the surface, which resulted in better activity towards methanol production. Using temperature programmed reduction (TPR), the addition of Ga in SBA-15 supported Cu catalysts was found to enhance the reducibility of the catalyst, resulting with a decrease of the reduction temperature from 267 °C for non-promoted Cu/SBA-15 to 250 °C for Ga promoted one(35). The study also found that Ga addition facilitates the formation of smaller

Cu particles (decreasing from 28 nm to 12 nm), and an increase in the catalyst surface area (24 to 46 m^2/g), resulting with an increase in the turnover frequency (TOF).

1.3.2.3   Holmium

Holmium as a promoter for CO_2 hydrogenation to methanol catalysts was first reported by Zohour et al.(33), where it was added to γ-Al_2O_3 supported Cu catalysts. Upon the application of a high-throughput experiment, they reported an increase of methanol production by a factor of two upon the addition to Cu-ZnO/γ-Al_2O_3, Cu-CeO_2/γ-Al_2O_3 and Cu-Ga/γ-Al_2O_3. On the other hand, for DME production, the addition of holmium resulted with more than two times increase in for Cu-ZnO/γ-Al_2O_3, while it showed about a 10−70 % decrease for both Cu-CeO_2/γ-Al_2O_3 and Cu-Ga/γ-Al_2O_3. STEM images suggest the creation of trimetallic sites, which is suggested upon the existence of 1−3 atom Ho clusters at the Cu and Ga cluster interfaces and on the surfaces of their alloys (5−7 nm), attributing that to the increase in the activity towards methanol production. Due to the lack of further experimental studies regarding holmium promotion, the actual effect imposed by holmium is yet to be thoroughly investigated. Through computational studies, however, Ho addition to Cu(211) surface is reported to strengthen the CO_2 binding as well as changing the reaction mechanism by stabilizing H_2COO^* intermediate rather than $HCOOH^*$ intermediate(36).

1.3.2.4   Lanthanum

The effect of La addition as a promoter has been studied in literature for Cu based catalysts by multiple scientists(37). Based on the results found by Zuo et al.(38), X-ray fluorescence results showed that the addition of La to phyllosilicate nanotube supported Cu, increased Cu dispersion. In addition, their CO_2-TPD results shows an increase in a desorption peak area upon the increase in La/Cu ratio, indicating an increase in the adsorption capacity of CO_2 with the addition of La. In addition, as

reported by Chou et al.(39), there is an increase in the adsorption strength of CO_2 upon the addition of La to In/ZrO_2 catalyst. This increase in CO_2 adsorption capacity and strength can attributed to the $Cu\text{-}LaO_x$ interfaces created through the interaction of Cu with LaO_x, as well as the tendency of La, being alkaline, to donate electrons, acting as a Lewis base site(40).

1.3.3   Catalyst Supports

1.3.3.1   Acidic Supports

In order to incorporate methanol dehydration reaction into the same system (onto the same catalyst), it is necessary to use bifunctional catalysts in order to further dehydrate methanol that is produced upon the hydrogenation of CO_2 on copper, into DME on another site. In such bifunctional catalysts, there must be acidic sites in order to dehydrate methanol to DME as dehydration reactions take place on them. The acidic sites tend to be those for the catalyst supports, such as $\gamma\text{-}Al_2O_3$ and zeolites. $\gamma\text{-}Al_2O_3$ contains Lewis acid sites due to the coordinatively unsaturated aluminum ions, acting as electron acceptors(41). Zeolites, on the other hand, possess both Brønsted and Lewis acid sites.

Zeolites are crystalline microporous aluminosilicates, with varying silicon and aluminum contents. When the zeolite framework is purely siliceous (Si/Al is infinity), it is neutrally charged. The decrease in the Si/Al ratio, however, causes an increase in the net negative charge in the framework, as $AlO_{4/2}$ replaces $SiO_{4/2}$. This negative charge has to be balanced by extra-framework cations such as Na^+, K^+, Mg^{2+} or protons (H^+) for stability. Presence of protons results in Brønsted acid sites(42). The Lewis acid sites, one the other hand, are developed from either extra-framework aluminum(43), or at the framework tetrahedral Al atoms(44). Hence, the Si/Al ratio is of a high importance in determining the acidity and the selectivity towards the production of DME(45). In order to determine the strength of the acid sites, NH_3 temperature programmed desorption (NH_3-TPD) is carried out, to result

with (mostly) three different peaks at three different temperatures, the highest being the strong acid sites and the lowest being the weak. There are many zeolites that can dehydrate methanol into DME, however, one of the well performing ones is ZSM-5 in terms of activity and selectivity(46). As was found in a study on ZSM-5(47), the weak and medium acid sites were responsible for the production of DME, while the strong ones were responsible for the production of other hydrocarbons, such as methane and ethylene.

1.3.3.2 Cerium

Multiple researches have been conducted over the effect of cerium addition to catalysts for CO_2 hydrogenation to methanol. Due to having more than one oxidation state, CeO_2 can be reduced from Ce^{4+} to Ce^{3+}, resulting with oxygen vacancies(48). Based on results found for Sm-doped CeO_2(49), there was a significant difference between the adsorbed CO_2 after reduction with H_2 (93.1 µmol/g) and after oxidation with O_2 (0.4 µmol/g), indicating that the creation of the oxygen vacancies facilitates the adsorption of CO_2. Based on a study by Wang et al.(50), it was observed that using CeO_2 as a support for Cu results with better dispersion and higher surface area, compared to ZrO_2. In addition, they observed that an XPS peak for pure CeO_2 is missing on Cu/CeO_2, as due to the metal support interactions, some Cu^{2+} ions were able to replace Ce^{4+}, to form more oxygen vacancies, as their corresponding XPS peaks appeared for Cu/CeO_2. It is suggested that CO_2 adsorbs onto the oxygen vacancy forming CO_2^{*}(51), or that it is adsorbed upon the reaction with the O^{2-} originated from the formation of the oxygen vacancies(50).

1.4 Other Catalysts

Other than Cu based catalysts, there has been some studies on Ni, Pd, In_2O_3 based catalysts. Silica supported Ni-Ga bimetallic catalysts showed a comparable performance (activity and selectivity) compared to $Cu/ZnO/Al_2O_3$(52). Unsupported

Pd-In bimetallic catalyst(53) and silica supported Pd-Cu bimetallic catalyst(54) showed higher methanol production compared to $Cu/ZnO/Al_2O_3$. However, when Pd is supported on acid supports, methane is produced as a major product. In_2O_3 is able to form oxygen vacancies due to the fact that indium has multiple oxidation states (+1, +3), which has already proven to increase activity towards synthesis of methanol over CeO_2 supported catalysts(55). In_2O_3 can actively both adsorb CO_2 and hydrogenate it to methanol, making it the only oxide catalyst that can achieve that(56). Reaction results of other catalysts and Cu based catalysts are shown in Table 1.1.

Table 1.1 Activity test results in literature for different catalysts under different conditions

Catalyst	T / °C	P / bar	r_{MeOH} / µmol g_{cat}^{-1} h^{-1}	r_{DME} / µmol g_{cat}^{-1} h^{-1}	S_{MeOH} / %	S_{DME} / %	X_{CO2} / %	Ref.
$Cu/ZnO/Al_2O_3$	260	331	241,230	-	77.3	-	66	(57)
$Cu/ZnO/Al_2O_3$	250	50	36,000	-	50	-	22	(58)
Cu/ZnO	210	1	36	-	12	-	0.8	(59)
Cu-Zn-Ga	270	30	4,242	-	29.7	-	15.9	(60)
$Cu-ZnO/ZrO_2$	240	30	1523	-	41.5	-	17	(61)
Pd-Cu	250	41	1116	-	34	-	6.6	(62)
$NiGa/SiO_2$	260	1	3901	-	-	-	-	(52)
In_2O_3	270	40	780	-	54.9	-	1.1	(56)
PdZn/ZSM-5	270	20	147	554	4.2	30.4	14	(63)
$Cu-Pd/CeO_2$	270	30	900	-	26.7	-	16.1	(64)
$CuNi_2/CeO_2$-NT	260	30	18100	-	78.8	-	17.8	(65)
Cu-Ga-Ho/ γ-Al_2O_3	260	1	-	-	24	14.7	-	(33)
Cu-LaO_x/ SBA-15	300	30	7803	-	62	-	-	(40)

1.5   CO₂ Hydrogenation to Methanol Mechanisms

CO_2 hydrogenation to methanol has been reported to take place through different mechanisms, which may depend on the catalyst of interest. In general, there are two suggested mechanisms that have been observed and reported in literature the most, which are the formate mechanism and rWGS+CO-Hydrogenation mechanism. In this section, both mechanisms will be explained briefly.

1.5.1   Formate mechanism

The hydrogenation of CO_2 to methanol via formate mechanism has been suggested in many DFT studies. The mechanism is initiated with CO_2 adsorption, which reacts with dissociated hydrogen atoms, firstly to form formate, then between formate and the final product, methanol, a lot of intermediates are formed such as formaldehyde (H_2CO^*) and methoxy (H_3CO^*). The suggested mechanism's intermediates in literature vary from one study to another. Figures 1.2-1.3 illustrate some of the suggested formate mechanisms reported in literature.
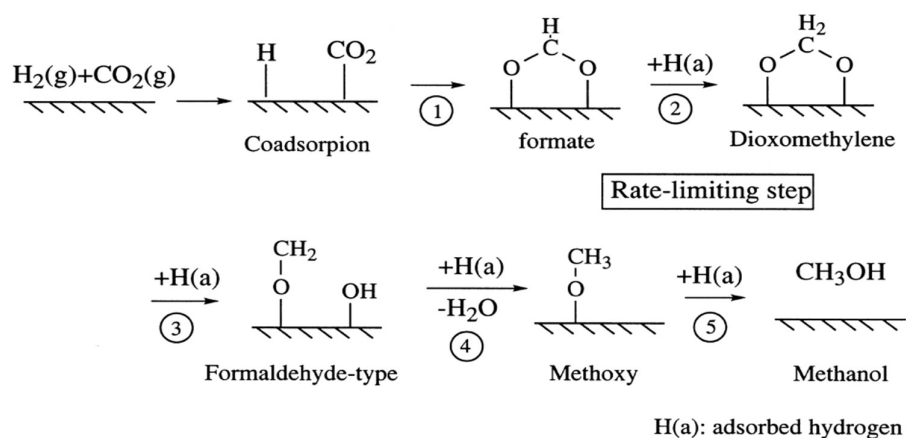
Figure 1.2 Proposed reaction mechanism of the hydrogenation of CO_2 to methanol on a Cu(100) surface(66)
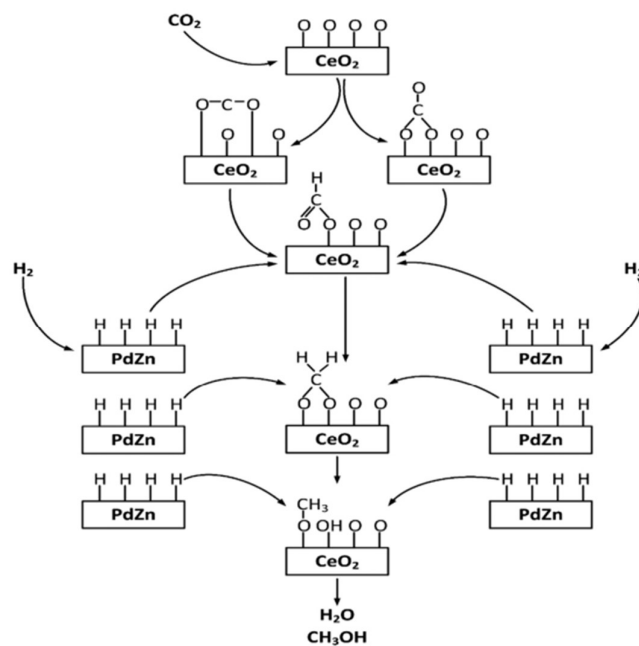
Figure 1.3 Proposed reaction mechanism of the hydrogenation of CO_2 to methanol over CeO2 supported Ca doped PdZn(67)

1.5.2   rWGS+CO-Hydrogenation Mechanism

As it was stated earlier, the rWGS reaction takes place parallel to methanol formation, causing lower selectivity of methanol. Some studies, however, were carried out to examine the feasibility of methanol to form upon the hydrogenation of the CO formed from the rWGS reaction. The formed CO was shown to favor desorption from Cu surface over hydrogenating to HCO* intermediate, resulting in production of CO as an undesired product. However, by doping with Ni, CO* energetically favors the direction of hydrogenating to HCO*, as it has a lower activation barrier compared to CO* desorption. The reaction then continues to form different intermediates till forming methanol. Another study on Cu/ZrO_2 showed a similar behavior. A schematic of the mechanism is shown in Fig. 1.4.
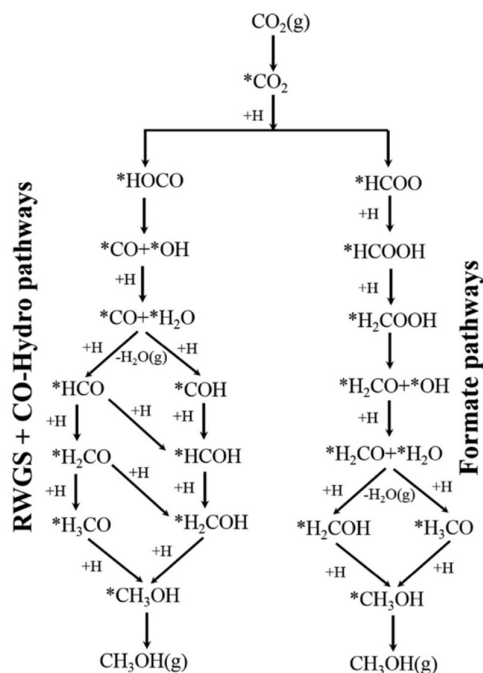
Figure 1.4 Proposed reaction mechanism of the hydrogenation of CO_2 to methanol via rWGS+CO hydrogenation pathway and formate pathway(68)

1.6 Objective

The aim of this study is to investigate the effect of different promoters (Ga, Ho and La) and supports (γ-Al_2O_3, ZSM-5 and CeO_2) on Cu based catalysts in the CO_2 hydrogenation to methanol and DME at the atmospheric pressure. It is aimed to load the catalysts with different combinations of promoters with different wt. %, and test their activity towards methanol and DME. In addition, operating conditions are also optimized by testing various temperatures, space velocities, and feed ratios. Characterization is also performed along with the activity tests, in order to better understand the lying factors in the different activities in different catalysts.

CHAPTER 2

EXPERIMENTAL PROCEDURE

2.1 Catalyst synthesis

In this thesis, γ-Al$_2$O$_3$, ZSM-5, and cerium oxide are used as supports for copper-based catalysts. ZSM-5 and cerium oxide are synthesized in the laboratory, while commercial γ-Al$_2$O$_3$ is purchased from Alfa-Aesar. After the synthesis of the supports, the catalysts are prepared via impregnation or coprecipitation-impregnation methods, where Cu, Ga, Ho, Zn and/or La are loaded on the support. The commercially used catalyst Cu/ZnO/Al$_2$O$_3$ is synthesized using coprecipitation for comparison. After the synthesis, the catalysts are reduced with hydrogen, after which the reaction is carried out.

2.1.1 Synthesis of H$^+$-ZSM-5

H$^+$-ZSM-5 is synthesized following a similar procedure reported by Mei et al.(69). At first, two mixtures are prepared separately in two separate beakers. The first mixture is composed of 49.922 g of HS-40 Ludox (Sigma Aldrich, 40 wt%) and 4.831 g of tetrapropylammonium hydroxide (TPAOH, Merck, 40 wt%), while the second one is composed of 0.44 g of sodium aluminate (Sigma Aldrich, 55% Al$_2$O$_3$, 44% Na$_2$O), 4.831 g of TPAOH (Merck, 40 wt%), and 17.668 g of de-ionized water. After stirring both of them separately for 30 mins at 25 °C, the second mixture is added drop wise to the first one, and the final suspension is kept stirring for 7 h at 25 °C. Afterwards, static hydrothermal synthesis is performed in Teflon-lined autoclaves at 180 °C for 5 days. Later, the formed zeolite particles are washed with de-ionized water and vacuum filtered, and then dried for 12 h in the oven at 60 °C.

Calcination is then carried out in a muffle furnace at 550 °C, after further drying at 120 °C for 1 h, using a heating rate of 1 °C/min. The calcined sample is then ammonium exchanged three times at 80 °C for 3 h, for a total of 9 h. Ammonium exchange is performed using a solution of ammonium nitrate (Merck, 99%) with a concentration of 0.2 M. After each time ammonium exchange is performed, it is followed by washing with de-ionized water and filtration and drying for 12 h. Lastly, a heat treatment is carried out at 550 °C for 5 h, after drying at 120 °C for 1 h, using a heating rate of 2 °C/min to obtain H^+-form of the zeolite.

2.1.2   Synthesis of CeO_2 Spheres.

CeO_2 spheres are synthesized following two different methods. The first method is reported by Tan et al. (65), 1.0 g of hexadecyl trimethyl ammonium bromide (ISO LAB, 97%) and 1.5 g of sodium acetate trihydrate (Merck, 99%) are added to 60 mL of ethyl glycol (Merck, 99.5%), then 2 g of cerium (III) nitrate hexahydrate (Sigma Aldrich, 99%) is dissolved in the suspension. The suspension is kept stirring at 300 rpm for 2 h until it is clear. Afterwards, it is transferred to a Teflon-lined autoclave and thermally treated in the oven at 180 °C for 4 h. The product is then cooled down to 25 °C, centrifuged and washed with ethanol. The product is then dried in the oven at 60 °C for 12 h. Calcination is then performed in a muffle furnace at 450 °C for 4 h, following drying at 120 °C for 1h, using a heating rate of 2 °C/min.

The second synthesis method is carried out as reported by Sun et al. (70). An amount of 0.01 mol of Glucose (Sigma Aldrich, 99%) is dissolved in 80 mL of de-ionized water, followed by the addition of 0.015 mol of acrylamide (Sigma Aldrich, 99%) and 0.005 mol of cerium nitrate hexahydrate (Sigma Aldrich, 99%). The solution is stirred for 5 min till a transparent solution is formed. Afterwards, 3.2 mL of ammonia (25%) is added to the solution drop wise, the resulting brown solution is further stirred for 5 h at room temperature. The solution is then transferred into an autoclave, and is then thermally treated in an oven at 180 °C for 3 days. The product is washed with water and ethanol, centrifuged and filtered. The resulting product is placed in

the oven to dry for 12 h at 60 °C. Calcination is then performed at 400 °C for 4 h, after drying at 120 °C for 1h, with a heating rate of 2 °C/min.

2.1.3 Synthesis of Cu/ZnO/Al₂O₃ by Coprecipitation

The Cu/ZnO/Al$_2$O$_3$ catalyst is synthesized by coprecipitation following the synthesis procedure reported by Baltes et al.(71). A catalyst with a weight ratio of 63Cu:33Zn:4Al is synthesized. At first, a solution of metal nitrate salts is prepared by dissolving copper nitrate tri-hydrate (Sigma Aldrich, ≥99.5%), zinc nitrate hexahydrate (Sigmal Aldrich, 99%), and aluminum nitrate nonahydrate (Merck, 95%) in de-ionized water resulting with a metal concentration of 1 M. As a precipitating agent, sodium carbonate (Merck, 99%) is used, where it is dissolved in de-ionized water resulting with a solution having a concentration of 1 M. Both solutions are then added separately to two different syringes, after which a syringe pump is used to pump both solutions simultaneously into an erlenmeyer flask containing de-ionized water. After the solutions are added, the mixture is left to age for 1 h. The precipitation and aging are both carried out at a temperature of 70 °C, a pH of 7 and stirring at 300 rpm. During precipitation and aging, sodium carbonate solution and diluted nitric acid are added dropwise, respectively, in order to maintain a constant pH of 7. The pH is measured throughout the synthesis with a pH probe (Mettler Toledo), which is also used to measure the temperature. The mixture is then washed with de-ionized water and vacuum filtered. The resulting product is then dried in oven at 60 °C for 12 h. Calcination is carried out in a muffle furnace at 300 °C for 4 hours, after drying at 120 °C for 1 h. The heating rate is set as 2 °C/min.

2.1.4 Metal Loading by Impregnation

The metals are added to the support materials using impregnation with a weight percentage of 10% for Cu, while for Ga, Ho, Zn, La and/or K, multiple weight percentages are used in a range of 1%-15%. Firstly, water is added to a beaker with

a ratio of 100 mL: 2 g support. Afterwards, copper nitrate tri-hydrate (Sigma Aldrich, $\geq 99.5\%$), gallium nitrate hydrate (Sigma Aldrich, 99.9%), holmium nitrate pentahydrate (Sigma Aldrich, 100%), zinc nitrate hexahydrate (Sigma Aldrich, 99%), Lanthanum nitrate hexahydrate (Sigma Aldrich, 100%), and/or potassium nitrate (Merck, 99%) are added to the de-ionized water. In order to ensure the dissolution of the metal nitrate salts, the beaker containing the solution is placed in an ultrasonic bath (ISO LAB) for 20 mins, followed by stirring at room temperature for 3 hours. The support is then added to the solution and the suspension is stirred at 300 rpm for 24 hours at 25 °C. In order to evaporate the water in the suspension, it is transferred to a round-bottom flask to undergo rotatory evaporation (IKA) at 20 rpm, 60 °C and 0.18 bar, until almost all of the water is evaporated and a paste is formed. The paste product is the is then placed in the oven to dry at 60 °C for 12 h. Finally, the dried product is calcined in a muffle furnace at 400 °C for 4 h, after drying at 120 °C for 1 h, using a heating rate of 2 °C/min.

2.1.5 Catalyst Synthesis by Coprecipitation-Impregnation

A catalyst having a weight ratio of $10Cu:5Ga:5Ho:100\gamma\text{-}Al_2O_3$ is synthesized by coprecipitation-impregnation. The synthesis method is identical to coprecipitation in every step, except that for coprecipitation-impregnation, the metal nitrate salts and sodium carbonate solutions are pumped simultaneously into an erlenmeyer flask containing $\gamma\text{-}Al_2O_3$ suspension, as opposed to only de-ionized water in coprecipitation. In addition, calcination is carried out at 400 °C, instead of 300 °C for coprecipitation.

2.2 Characterization Techniques

The catalyst characterization is performed using multiple techniques. Powder X-ray Diffraction (XRD) to identify existing phases and quantifying crystal sizes. Transmission electron microscopy (TEM) to capture images of the catalysts for

particle size determination. N_2 adsorption/desorption at -196 °C to quantify the surface area of the catalyst. Inductively coupled plasma optical emission spectroscopy (ICP-OES) to quantify the elemental composition of the synthesized catalysts. Temperature programmed reduction (TPR) to estimate the catalyst dispersion. Temperature programmed desorption (TPD) to quantify the basic sites.

2.2.1 X-Ray Diffraction (XRD) Analysis

X-ray diffraction analysis is carried out for the catalyst after synthesis, as well as after reduction with H_2 (50 %) at 250 °C for 2 h and 100 sccm. The analysis is performed using Rigaku Ultima IV diffractometer, with a K-α Cu X-ray source (λ=1.5418 Å) operating at 40 kV and 30 mA. The diffractogram is obtained for the 2θ angles of 10–80 ° with a scanning speed of 1 °/ min at Central Laboratory, METU. From the diffractogram obtained, the existing phases determined, and the size of the crystals (d_c) are calculated using Scherrer equation (Eq. 2.1), where β is full width at half maximum (FWHM), and K is taken as 0.9.

$$d_c = \frac{K\lambda}{\beta cos\theta}$$
Eq. 2.1

2.2.2 Transmission Electron Microscopy (TEM) Analysis

Transmission electron microscopy analysis is performed on reduced samples, in order to estimate the particle sizes using ImageJ program. The analysis is carried out using JEOL-Jem 2100 TEM, operating at an accelerating voltage of 200 kV.

2.2.3 N_2 Adsorption/Desorption

N_2 adsorption/desorption is performed in order to obtain the pore volume and surface area of the catalysts, using Micromeritics Tristar II 3020 pore volume and surface area analyzer, in the Department of Chemical Engineering, METU. Prior to N_2

adsorption, the catalyst is degassed for 6 h at 300 °C and 0.15 bar using Micromeritics VacPrep 061. N_2 adsorption/desorption is carried out at -196 °C and N_2 (Oksan, 99.999%) at relative pressure (P/P_0) values between 10^{-5} and 0.99.

2.2.4   Inductively Coupled Plasma Optical Emission Spectroscopy (ICP-OES) Analysis

Inductively coupled plasma optical emission spectroscopy (ICP-OES) analysis is carried out in Central Lab, METU, to obtain the elemental composition of the catalysts synthesized, and compare it with the theoretical values. Prior to the analysis, the catalysts are dissolved in nitric acid or hydrofluoric acid.

2.2.5   Temperature Programmed Reduction (TPR) Analysis

Temperature programmed reduction is carried out by first reducing the catalyst ($\sim$ 50 mg) with H_2 flow (15%, total flow rate $\sim$ 60 sccm) while heating it up to 500 °C, starting from 25 °C, using a heating rate of 10 °C/min. The data regarding the detected H_2 signals are recorded simultaneously using Mass Spectrometer (HIDEN HPR20). Afterwards, N_2O chemisorption is carried out at 60 °C for 1 h to oxidize the surface of the catalyst. Lastly, Reduction is carried out again with the same conditions, and the results are again reported simultaneously using Mass Spectrometer (HIDEN HPR20). The area of the resulting curves of the consumption of hydrogen are estimated, and the dispersion is then determined. The H_2-TPR+N_2O process takes place as shown in Eq. 2.2-2.4:

$$CuO + H_2 \rightarrow Cu + H_2O \qquad\qquad\qquad\qquad\qquad \text{Eq. 2.2}$$

$$2Cu + N_2O \rightarrow Cu_2O + N_2 \qquad\qquad\qquad\qquad\qquad \text{Eq. 2.3}$$

$$Cu_2O + H_2 \rightarrow 2Cu + H_2O \qquad\qquad\qquad\qquad\qquad \text{Eq. 2.4}$$

where the first reaction corresponds to the 1st TPR step, where each H_2 corresponds to one Cu site, whilst for the last step (2nd TPR, after N_2O chemisorption) each H_2 molecule corresponds to 2 Cu sites. Hence, the dispersion is calculated as shown in Eq. 2.5 based on the areas for the first (A_1) and second (A_2) TPR. Based on the dispersion results, particle size is calculated as shown in Eq. 2.6, where M is the molecular weight of copper, σ is the area occupied by a surface Cu atom, ρ is the density of methanol, and N_0 is Avogadro's number.

$$D = 2\frac{A_2}{A_1} \times 100\% \qquad\qquad\qquad\qquad\qquad \text{Eq. 2.5}$$

$$d_p = \frac{6M}{D\rho\sigma N_0} \qquad\qquad\qquad\qquad\qquad \text{Eq. 2.6}$$

2.3 Catalytic Test of CO_2 hydrogenation to methanol.

2.3.1 Reduction with H_2

The catalyst is placed in a borosilicate reactor of 7 mm inner diameter and 9 mm outer diameter using glass wools to stabilize the catalyst in a packed bed reactor. As the reaction is carried out at elevated temperatures, the reactor is placed inside of a tubular furnace. Prior to the reaction, reduction of the catalysts is performed using equimolar flow of hydrogen gas (Hatgaz, 99.999%) and helium gas (Hatgaz, 99.999%) with a total volumetric flow rate of 100 sccm for 2 h at 250 °C (using a heating rate of 5 °C/min). Both gases are sent through stainless steel lines (Swagelok 1/8") to mass flow controllers (Alicat Scientific) to adjust the flow, after which they get mixed at a mixing point before being fed to the reactor.

2.3.2 Reaction Procedure

After the reduction is completed, and as the oven temperature is cooling down to the reaction temperature, helium is flushed in the reactor for 20 minutes to ensure the removal of the chemisorbed hydrogen on the catalyst surface. Following the cooling of the reactor, the gas flow is adjusted using the mass flow controllers (Alicat Scientific) to determined ratios of H_2 and CO_2 ($3H_2:1CO_2$, $6H_2:1CO_2$, and $9H_2:1CO_2$) with a total flow rate of 100 sccm without any inert addition, and the reaction is carried out at the determined reaction temperature (200, 220 and 240 °C). In addition, different gas hourly space velocities (GHSV) of 25,000, 10,000, and 7,000 h^{-1} are tested, achieved by loading the reactor with 200, 500 and 700 mg of catalyst (m_{cat}).

The products are analyzed every 30 minutes using a gas chromatography (GC, Agilent 7890B), where auto-sampling is performed online using stainless steel lines (Swagelok 1/8") connecting between the exit of the reactor and entrance of the GC. In order to prevent the condensation of methanol and water, the stainless-steel lines (Swagelok 1/8") connecting the lines are heated up to 100 ℃. Data for each reaction condition is taken until steady state is reached. The product analysis is performed using a GC equipped with a GS-CarbonPLOT column of 30m length, 0.32mm diameter and 3μm film thickness, a flame ionization detector (FID), a thermal conductivity detector (TCD) and a methanizer. Process flow diagram of the reaction setup can be seen in Fig. 2.1.
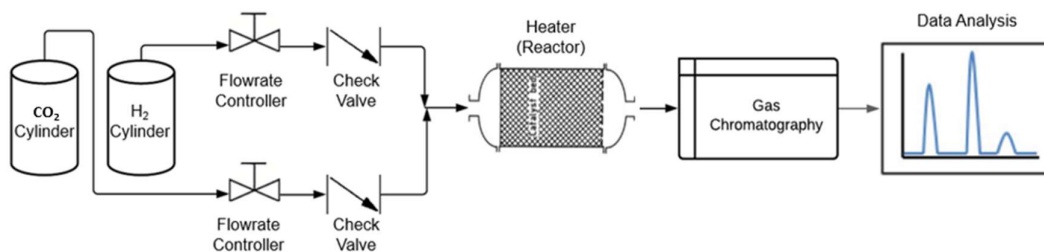
Figure 2.1 Process flow diagram of the reaction setup

To obtain the conversion of CO_2, a blank reactor is run with the same feed ratio, so as to be able to determine the fraction of the CO_2 in the feed. The products (MeOH, DME, and CO) selectivity (S) and CO_2 conversion (X) are calculated by means of the formation rates (r) and molar flowrates (F), as shown in Eq. (2.7) and (2.8). The subscript "i" stands for the products, and "c" for the number of carbon atoms per molecule. The formation rate is calculated based on the ideal gas equation, where the parameters are the total volumetric flowrate measured at the exit of the GC (v_{total}), temperature (T) and pressure (P) of the surroundings, the response factor of the corresponding product (f_r), the area of the peak of the corresponding product (A), and the weight of the catalyst (m_{cat}), as shown in Eq. 2.9.

$$S_i = \frac{c_i\, r_i}{\Sigma_i\, c_i r_i} \qquad\qquad \text{Eq. 2.7}$$

$$X_{CO_2} = \frac{\Sigma_i\, c_i r_i}{F_{CO_{2_{inlet}}}/m_{cat}} \qquad\qquad \text{Eq. 2.8}$$

$$r_{MeOH} = \frac{v_{total}Pf_r A}{RTm_{cat}} \qquad\qquad \text{Eq. 2.9}$$

CHAPTER 3

RESULTS AND DISCUSSION

3.1 Characterization Results

3.1.1 ICP-OES

ICP-OES analysis is carried out to obtain the resulting elemental content of each of the synthesized catalysts. As can be observed from Table 3.1., the theoretical loading and the actual loading values were close for Cu. For Ho, Zn and especially Ga, however, the actual value was less than the theorical ones.

Table 3.1 Elemental analysis by ICP-OES of some of the synthesized catalysts

Catalyst	Cu / %	Ga / %	Ho / %	Zn / %	La / %
10Cu-10Ga/γ-Al$_2$O$_3$	8.7	5.5	-	-	-
10Cu-12Ga/γ-Al$_2$O$_3$	8.7	7.1	-	-	-
10Cu-15Ga/γ-Al$_2$O$_3$	8.5	8.4	-	-	-
10Cu-5Ga-1La//γ-Al$_2$O$_3$	9.3	3.2	-	-	0.97
10Cu-10Ho//γ-Al$_2$O$_3$	9.1	-	8.2	-	-
10Cu-10Zn/γ-Al$_2$O$_3$	8	-	-	7.7	-
10Cu/CeO$_2$	9.1	-	-	-	-
10Cu-5Ga/CeO$_2$	8.4	3	-	-	-
10Cu-5Ga-1La/CeO$_2$	8.4	2.9	-	-	0.85

3.1.2   XRD

XRD analysis is caried out to identify the existing metal/metal oxides phases in the catalyst, as well as to obtain the copper crystal sizes. Data recorded are in a 2θ range of 10–80°. Fig. 3.1 shows that there is a noticeable effect upon the addition of Ho, resulting in sharper peaks of Cu in Ho (10%) containing catalyst, compared to the broad peaks for Ga (5% and 10%) containing ones. Difference between γ-Al_2O_3 and H^+-ZSM5 supported 10Cu-5Ga-5Ho can be seen in Fig. 3.2, where no Cu phase is detected for γ-Al_2O_3 as opposed to sharp Cu phase peaks for H^+-ZSM5. Like Ho, Zn containing samples show sharp Cu peaks, as shown in Fig. 3.3. It is also observed that the most commonly appearing Cu phase is Cu (111). Cu (200) and Cu (220) phases are observed on Zn and Ho containing catalysts. It is important to note that the remining peaks correspond to the supports.
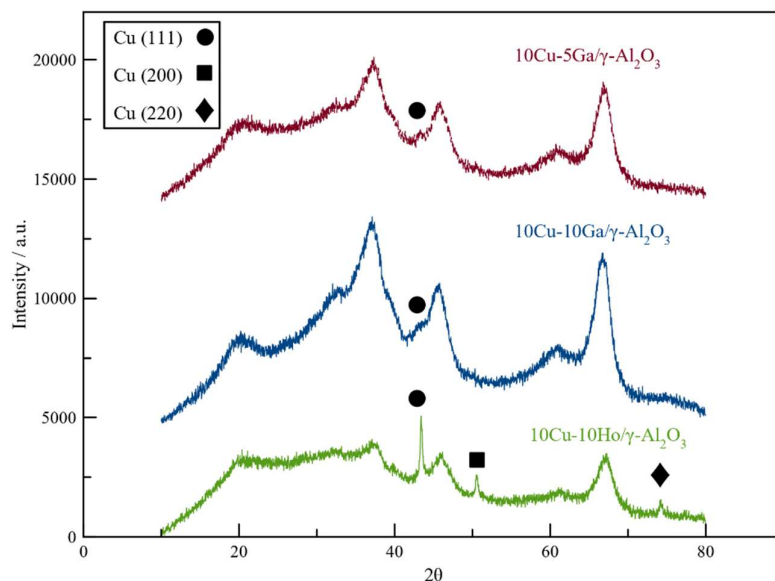
Figure 3.1 XRD pattern for γ-Al_2O_3 supported, Cu-Ga and Cu-Ho catalysts, remaining peaks correspond to Al_2O_3 (λ=1.5418 Å)

26
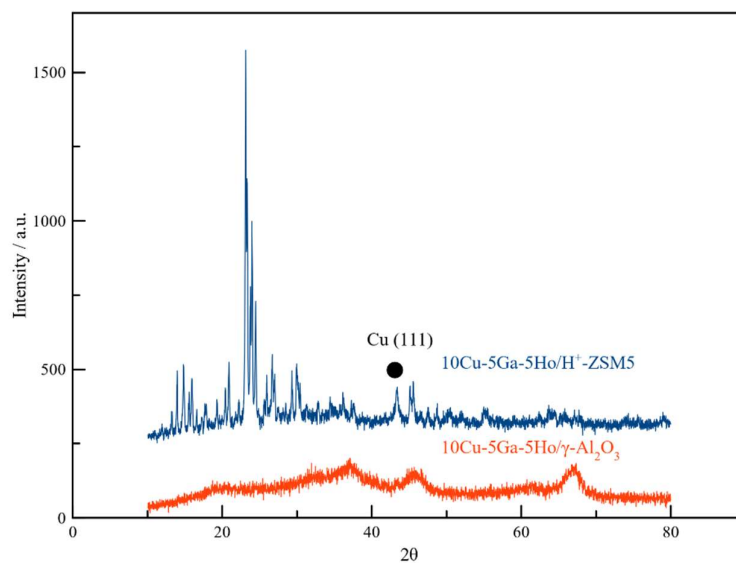
Figure 3.2 XRD pattern for γ-Al$_2$O$_3$ and H$^+$-ZSM-5 supported Cu-Ga-Ho catalysts, remaining peaks correspond to Al$_2$O$_3$ and H$^+$-ZSM-5 (λ=1.5418 Å)
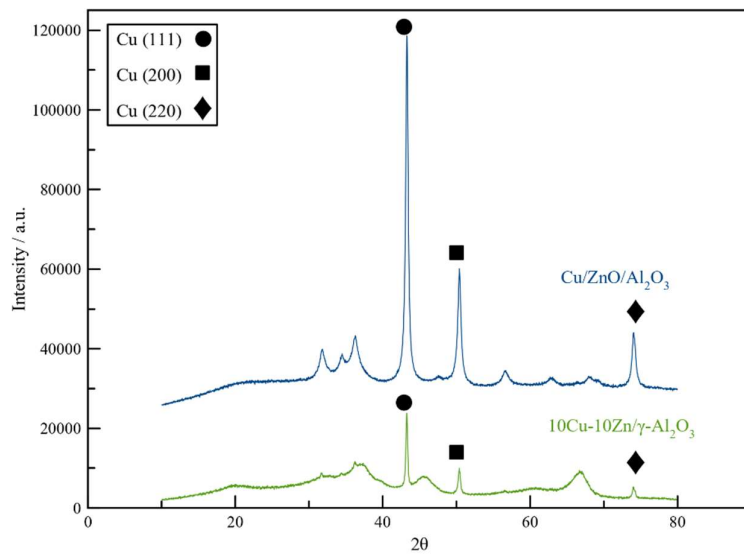
Figure 3.3 XRD pattern for Cu/ZnO/Al$_2$O$_3$ and 10Cu-10Zn/γ-Al$_2$O$_3$, remaining peaks correspond to Al$_2$O$_3$ (λ=1.5418 Å)

Even though the detection of peaks and their broadening or sharpness can give qualitative results, it is necessary to have quantitative ones to have a better comparison. Hence, Scherrer equation (Eq. 2.1) is applied. Results of some of the synthesized catalysts' Cu(111) crystal sizes are reported in Table 3.2. Remaining XRD patterns of the samples are given in Figure A.1-A.3. It is observed that CeO_2 synthesized following different synthesis methods resulted in larger Cu crystals for the 1st synthesis method. It is clear that Cu-Ga/γ-Al_2O_3, as was seen in the Fig. 3.1, have the smallest crystal sizes, as opposed to Ho and Zn ones.

Table 3.2 Crystal sizes of Cu(111) found by Scherrer equation

Catalyst	d_c / nm
10Cu-5Ga/γ-Al_2O_3	4
10Cu-10Ga/γ-Al_2O_3	3
10Cu-5Ga-1La/γ-Al_2O_3	13
10Cu-10Ho/γ-Al_2O_3	50
10Cu-5Ga-5Ho/γ-Al_2O_3	-
10Cu-10Zn/γ-Al_2O_3	40
10Cu-10Ga/H^+-ZSM5	16
10Cu-10Ho/H^+-ZSM5	15
10Cu-5Ga-5Ho/H^+-ZSM5	26
10Cu/CeO_2 (2nd)	18
10Cu-5Ga/CeO_2 (1st)	35
10Cu-5Ga/CeO_2 (2nd)	26
10Cu-5Ga-1La/CeO_2 (2nd)	13
10Cu-5Ga/SiO_2	24
Cu/ZnO/Al_2O_3	26

Similar to CeO_2, it is observed that different metal loading techniques over the support affects Cu crystal size, as in the case for 10Cu-5Ga-5Ho/γ-Al_2O_3, as the

coprecipitation-impregnation method results in detectable CuO crystal phases with crystal size of 12 nm, while impregnation does not, as can be seen in Fig 3.4.
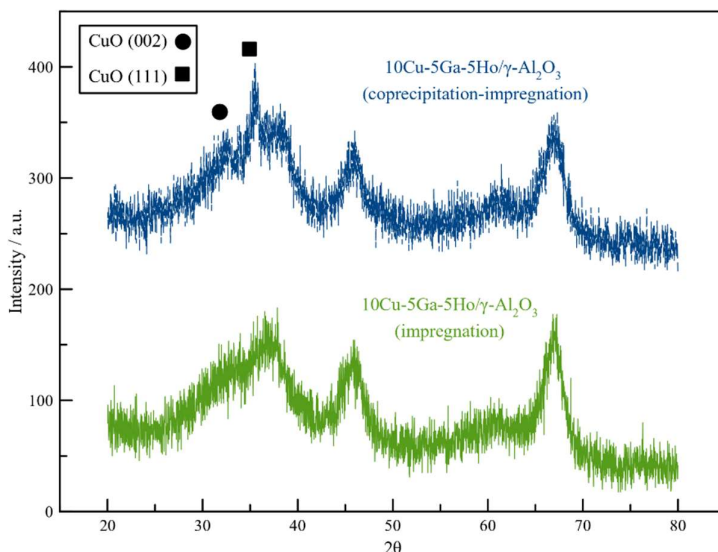
Figure 3.4 XRD pattern of unreduced Cu-Ga-Ho/γ-Al$_2$O$_3$ synthesized via impregnation and coprecipitation-impregnation, remaining peaks correspond to Al$_2$O$_3$ (λ=1.5418 Å)

In an attempt to determine the existence of Cu-Ga or Cu-Ho alloys, 2θ values of Cu (111) for promoted and unpromoted Cu/γ-A$_2$lO$_3$ are reported for comparison in Table 3.3. As can be seen, 10% Ga promoted and 5% Ho promoted ones show almost a similar 2θ, where 5% Ga promoted one show a slightly different 2θ than the unpromoted catalyst, which may possibly indicate a Cu-Ga alloy formation.

Table 3.3 2θ values of Ga and Ho promoted Cu/γ-Al$_2$O$_3$

Catalyst	2θ of Cu (111) / °
10Cu/γ-Al$_2$O$_3$	43.30
10Cu-5Ga/γ-Al$_2$O$_3$	43.07
10Cu-10Ga/γ-Al$_2$O$_3$	43.28
10Cu-5Ho/γ-Al$_2$O$_3$	43.42

3.1.3   N$_2$ Adsorption/Desorption

The surface areas of the synthesized catalyst are obtained and reported in Table 3.4. As can be seen, H-ZSM5 supported catalysts have the 2nd highest BET surface areas, after silica. However, it has the lowest external surface area, compared to γ-Al$_2$O$_3$ and SiO$_2$ supported ones, which may explain the larger crystals formed on ZSM-5 supported catalyst. It is also observed that the total and external surface areas of Cu-Ga/CeO$_2$ are higher for the one synthesized in the 2nd method, which may explain the smaller Cu crystals formed on it, as opposed to the 1st method. As shown in Table 3.3, despite the larger surface area found on SiO$_2$ compared to γ-Al$_2$O$_3$, γ-Al$_2$O$_3$ supported 10Cu-5Ga catalyst had smaller crystals, which may be due to the difference between SiO$_2$ and γ-Al$_2$O$_3$ in their interaction with Cu.

Table 3.4 BET, Langmuir, t-plot external and micropore surface area for different catalysts

Catalyst	SA$_{BET}$ / m^2 g^{-1}	SA$_{Langmuir}$ / m^2 g^{-1}	SA$_{external.}$ / m^2 g^{-1}	SA$_{micropore.}$ / m^2 g^{-1}
10Cu-10Ga/γ-Al$_2$O$_3$	143	197	126	16
10Cu-10Ho//γ-Al$_2$O$_3$	132	182	115	17
10Cu-5Ga/CeO$_2$ (1st)	50	69	37	32
10Cu-5Ga/CeO$_2$ (2nd)	94	128	90	37
10Cu-10Ga/H-ZSM-5	286	390	82	204
10Cu-10Ga/SiO$_2$	244	338	218	120
Cu/ZnO/Al$_2$O$_3$	64	87	60	27

3.1.4   TEM Images

TEM images are recorded in order to obtain the particle size distribution of Cu in some of the catalysts, including 10Cu-10Ga and 10Cu-10Ho supported on γ-Al$_2$O$_3$

and H^+-ZSM-5. Cu particle sizes are recorded and their distribution is shown in Fig. 3.5. As can be observed from TEM images, γ-Al_2O_3 supported catalysts showed better dispersion and uniform distribution over the support, as opposed to H^+-ZSM-5 supported ones. Quantification of the Cu particles shows that indeed γ-Al_2O_3 supported catalysts have smaller particle size distribution than H^+-ZSM-5 supported ones, especially for 10Cu-10Ga/γ-A_2lO_3, having an average of 4 nm particles, which agrees with the crystal size calculated from XRD results. However, compared to XRD, 10Cu-10Ho/ γ-Al_2O_3 shows smaller average particle size of 5 nm (ranging between 3 and 14 nm), as opposed to about as high as 50 nm from XRD. This could be due to the existence of other larger particles that are not seen or recorded for the analyzed region in TEM.
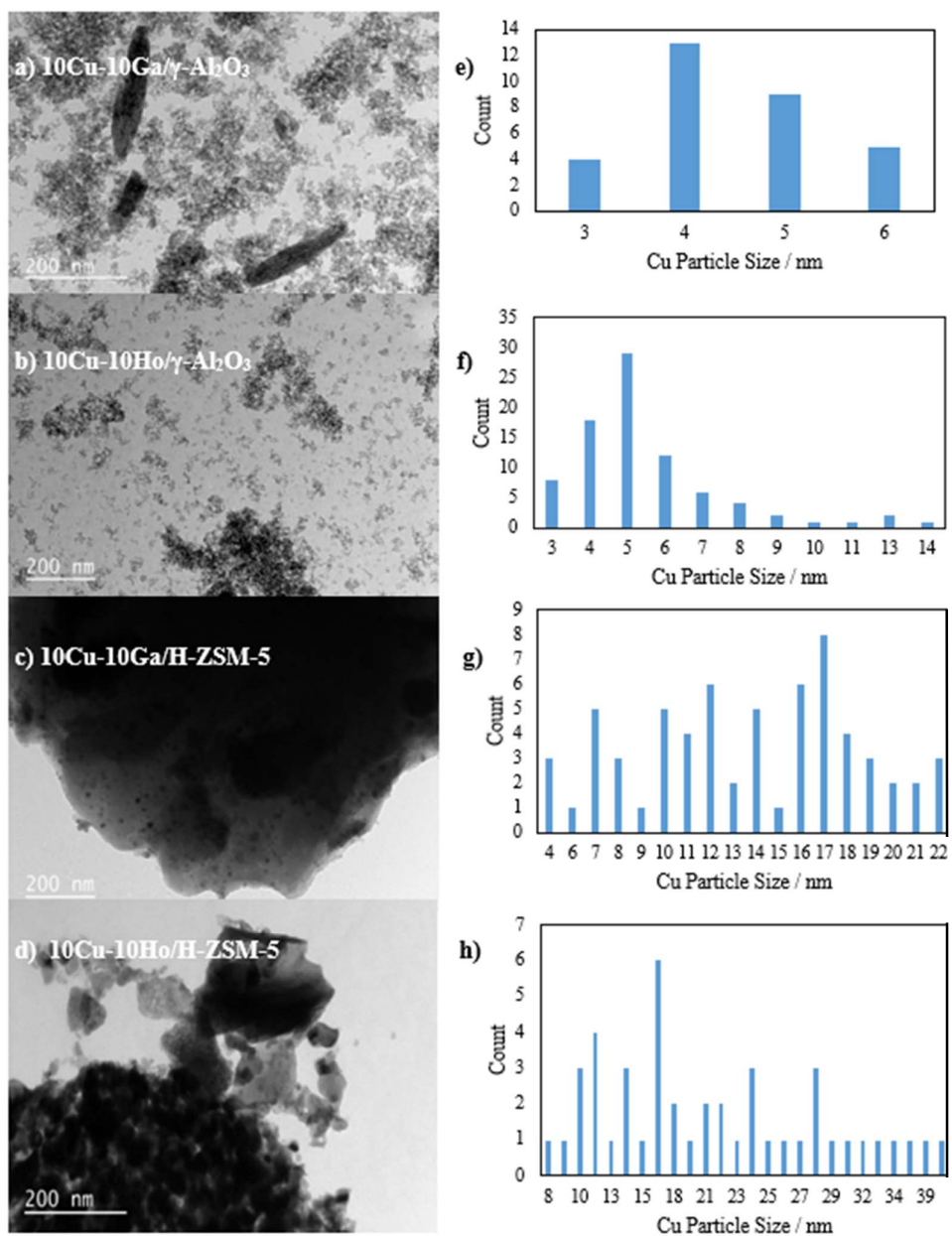
Figure 3.5 TEM images of a) 10Cu-10Ga/γ-Al$_2$O$_3$, b) 10Cu-10Ho/γ-Al$_2$O$_3$, 10Cu-10Ga/H$^+$-ZSM-5 and 10Cu-10Ho/H$^+$-ZSM-5, and their corresponding Cu particle distribution e), f), g) and h), respectively.

3.1.5   TPR

A procedure including two H_2-TPR and one N_2O adsorption experiment was employed to be able to quantify the total Cu amount as well as the surface Cu amount. As mentioned previously, H_2-TPR is carried out twice, once before (bulk reduction) and once after (surface reduction) N_2O chemisorption. An example of one of the TPR graphs is shown in Fig 3.6. Based on the resulting areas of both TPRs, the dispersion is calculated from Eq. 2.5 and reported in Table 3.5. It is observed that dispersion is found lower in the catalysts containing Ho, while it was higher for those containing Ga. The particle size estimation by Eq. 2.6 using the dispersion percentage found from TPR measurements are lower than the ones found via TEM and XRD (see Table 3.4). However, the trend based on the dispersion and particle size is consistent with that found in both TEM and XRD, where Ga containing catalysts has smaller crystals and particles.
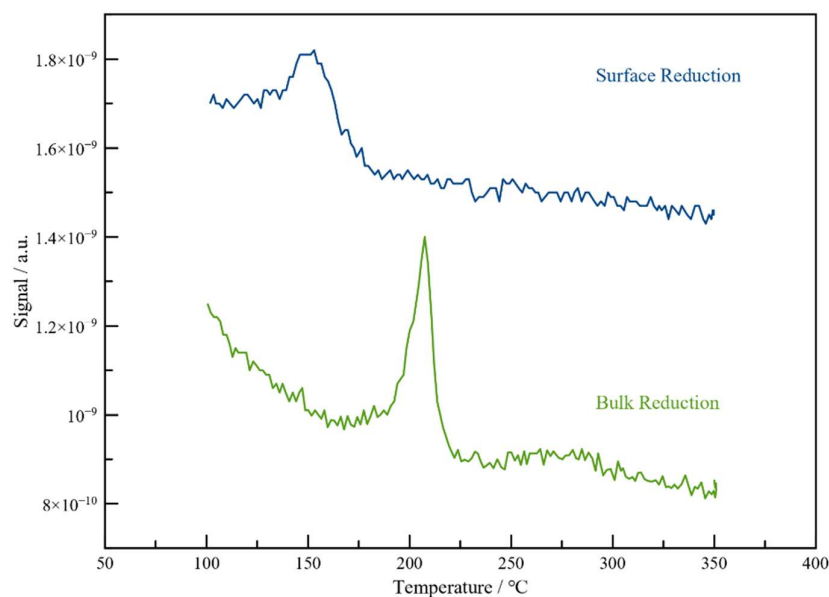
Figure 3.6 TPR of 10Cu-10Ga/γ-Al$_2$O$_3$ after bulk reduction (prior to N_2O chemisorption) and after surface reduction (after N_2O chemisorption)

Table 3.5 Dispersion percentage found by TPR for γ-Al$_2$O$_3$ supported Cu-Ga and Cu-Ho and their corresponding Cu particle sizes

Catalyst	D / %	d_p / nm
10Cu-5Ga/γ-Al$_2$O$_3$	61	1.7
10Cu-10Ga/γ-Al$_2$O$_3$	70	1.5
10Cu-10Ho/γ-Al$_2$O$_3$	52	2.0

3.2   Activity Tests

Different catalysts have been prepared using different techniques, as well as different promoters and supports. The prepared catalysts are tested under different conditions, in order to achieve the highest yield and selectivity of methanol and DME. In this section, the major results regarding the activity tests for different catalysts and conditions are reported.

3.2.1   Effect of Different Metal Loading Techniques

Two different metal loading techniques, which are impregnation and coprecipitation-impregnation, were applied to prepare 10Cu-5Ga-5Ho/γ-Al$_2$O$_3$ catalysts. Results of the activity tests are shown in Table 3.6. It can be observed that the coprecipitation-impregnation loaded catalysts resulted with higher yield for all of the products, compared to impregnation. However, it resulted with a lower selectivity of both methanol and DME, meaning that the CO is increased more than methanol and DME. XRD spectra shown in Fig 3.4 shows how larger particle sizes are likely to exist on the coprecipitation-impregnation loaded catalysts. Hence, this higher activity and lower selectivity observed on it compared to impregnation loaded catalyst, may be attributed to the larger particle size. Compared to impregnation, coprecipitation-impregnation technique imposes a difficulty in replicating the same procedure, due to the continuous temperature and pH fluctuations during coprecipitation and aging.

Such challenges may result with less homogeneity of particle size distribution(72). These difficulties may cause an error in examining the effect of promoters, as the effect of a promoter may be mistaken to inconsistent experimental parameters during the process. Impregnation, on the other hand, requires less effort in terms of maintaining constant parameters during the process, resulting with better particle size distribution, as well as allowing the replication of the method over again (illustrated in section 3.2.6).

Table 3.6 Activity test results for 10-5Ga-5Ho/γ-Al$_2$O$_3$ synthesized with different preparation methods. Activity tests conducted at 220 °C, 25,000 h^{-1} and 9H$_2$/1CO$_2$

Prep. Method	r_{MeOH} / μmol g_{cat}^{-1} h^{-1}	r_{DME} / μmol g_{cat}^{-1} h^{-1}	r_{CO} / μmol g_{cat}^{-1} h^{-1}	S_{MeOH} / %	S_{DME} / %	S_{CO} / %	X_{CO2} / %
Imp.	53.2	7.4	1213.5	4.2	1.1	94.7	1.2
Copr.-Imp.	89.7	13.1	2395.8	3.6	1.0	95.4	2.2

In addition, two calcination temperature are examined, which are 350 and 400 °C and the results can be seen in Table 3.7. As can be seen, there is a slight increase in methanol yield of methanol and DME, with an almost equal selectivity. The 50 °C difference in temperature may be responsible of a slight increase of particle size for the catalyst calcined at 400 °C. In the following sections, all of the results reported are for catalysts loaded using impregnation and calcined at 400 °C, unless otherwise mentioned. Note that the coprecipitation technique is not mentioned here, as this is only used for the replication of the commercial catalyst Cu/ZnO/Al$_2$O$_3$.

Table 3.7 Activity test results for 10-5Ga-5Ho/γ-Al$_2$O$_3$ metal loaded via impregnation and calcined at 350 and 400 °C. Activity tests conducted at 220 °C, 25,000 h^{-1} and 9H$_2$/1CO$_2$

$T_{calcination}$ / °C	r_{MeOH} / $\mu mol\ g_{cat}^{-1}h^{-1}$	r_{DME} / $\mu mol\ g_{cat}^{-1}\ h^{-1}$	r_{CO} / $\mu mol\ g_{cat}^{-1}\ h^{-1}$	S_{MeOH} / %	S_{DME} / %	S_{CO} / %	X_{CO2} / %
350	47.0	5.3	1027.9	4.3	1.0	94.7	1.0
400	53.2	7.4	1213.5	4.2	1.1	94.7	1.2

3.2.2 Optimization of Reaction Conditions

Different reaction conditions, including temperature, feed ratio, as well as space time velocity were tested, one parameter at a time, in order to conduct the reaction under optimal conditions.

3.2.2.1 Temperature

Most of the catalysts are tested under different temperatures, mostly at 200, 220, and 240 °C. The results of the activity tests of some of the catalysts are shown in Table 3.8. As can be seen, the increase of the reaction temperature increases the conversion of CO$_2$ to methanol, DME and CO. It is apparent that operating at higher temperatures results in higher selectivity of CO compared to lower temperatures, which is expected due to the endothermicity of the reverse water gas shift reaction. The results suggest that even though the reaction is operating in the kinetic region, which is indicated by the low CO$_2$ conversion, it is not possible to ignore the thermodynamics of the reactive system, where temperature has a direct impact on the system favoring CO formation at higher temperatures. It is important to note that the CO$_2$ thermodynamic conversions at 200, 220 and 240 °C are all above 10%(73), hence, in our case, the reaction is far from equilibrium, and under kinetic control.

Table 3.8 Activity test results for different catalysts at different reaction temperatures at 25,000 h^{-1} and 9H$_2$/1CO$_2$

Catalyst	T / °C	r_{MeOH} / μmol g$_{cat}^{-1}$ h^{-1}	r_{DME} / μmol g$_{cat}^{-1}$ h^{-1}	r_{CO} / μmol g$_{cat}^{-1}$ h^{-1}	S_{MeOH} / %	S_{DME} / %	S_{CO} / %	X_{CO2} / %
10Cu-	200	26.6	27.7	316.7	6.7	13.9	79.4	0.3
10Ga/	220	41.6	42.3	926.5	4.0	8.0	88	0.7
γ-Al$_2$O$_3$	240	62.2	43.9	2132.9	2.7	3.9	93	1.4
10Cu-	200	39.6	1.9	441.7	8.2	0.8	91.0	0.3
10Ho/	220	67.8	4.9	1253.0	5.1	0.7	94.2	0.8
γ-Al$_2$O$_3$	240	81.8	7.1	2988.2	2.7	0.5	96.8	1.9
10Cu-	200	91.0	0.6	682.8	11.7	0.2	88.1	0.5
10Zn/	220	139.8	1.1	2069.3	6.3	0.1	93.6	1.3
γ-Al$_2$O$_3$	240	147.2	1.4	5568.9	2.5	0.1	97.4	3.5

3.2.2.2   H$_2$/CO$_2$ Feed Ratio

Feed ratio (H$_2$/CO$_2$) values of 9/1, 6/1, and 3/1 were tested and results of some of the catalysts are shown in Table 3.9. As can be observed, feed ratio of 9/1 resulted with the highest methanol selectivity in line with literature(57,73), due to having the lowest CO yield. Methanol also showed a decrease in yield, while DME showed a slight increase, as the feed ratio increased from 3/1 to 9/1. Contrary to what is found in these catalytic tests, in literature, higher methanol formation is found on higher H$_2$/CO$_2$ ratios. In addition, there is an increase in the CO$_2$ conversion at higher feed ratios, as it is according to thermodynamics, CO$_2$ becomes a limiting reactant at ratios above 3/1.

Table 3.9 Activity test results for 10Cu-10Ga/γ-Al$_2$O$_3$ and 10Cu-10Ho/γ-Al$_2$O$_3$ at different feed ratios at 220 °C and 25,000 h^{-1}

Catalyst	H$_2$/CO$_2$	r_{MeOH} / μmol $g_{cat}^{-1}h^{-1}$	r_{DME} / μmol $g_{cat}^{-1}h^{-1}$	r_{CO} / μmol $g_{cat}^{-1}h^{-1}$	S_{MeOH} / %	S_{DME} / %	S_{CO} / %	X_{CO2} / %
10Cu-	3/1	42.6	33.0	1324.2	3.0	4.6	92.4	0.4
10Ga/	6/1	37.1	36.0	1019.4	3.3	6.4	90.3	0.4
γ-Al$_2$O$_3$	9/1	33.2	35.6	842.0	3.5	7.5	89.0	0.6
10Cu-	3/1	69.8	3.5	1667.7	4.0	0.4	95.6	0.5
10Ho/	6/1	69.2	4.4	1319.4	5.0	0.6	94.4	0.6
γ-Al$_2$O$_3$	9/1	63.4	4.8	1176.7	5.1	0.8	94.1	0.8

3.2.2.3   Space Time Velocity

Activity test results for different space time velocities applied on 10Cu-10Ga/γ-Al$_2$O$_3$ are shown in Table 3.10. It is observed that the increase in GHSV from 7,000 h^{-1} to 10,000 h^{-1} results with an increase in the activity towards the three products. The increase in GHSV from 10,000 h^{-1} to 25,000 h^{-1} results with a slight decrease in CO yield and an increase in methanol and DME yield. In terms of selectivity, upon the increase in GHSV, the selectivity of methanol and DME increased, while that for CO decreased. It is possible that this trend is observed due to the difference in oxygen coverage upon applying different GHSV, as found by Lee et al. (74). According to their findings, different GHSV values results with different oxygen coverage, which affects the conversion of CO$_2$ to methanol and CO rates, resulting with a similar trend found in Table 3.9. Also, faster kinetics of methanol formation with respect to CO formation favors higher GHSV(75). Based on the results found, GHSV of 25,000 h^{-1} is considered to be the optimal one in this study.

Table 3.10 Activity test results for 10Cu-10Ga/γ-Al$_2$O$_3$ at different GHSV at 220 °C and 9H$_2$/1CO$_2$

GHSV / h^{-1}	r$_{MeOH}$ / μmol g$_{cat}^{-1}$ h^{-1}	r$_{DME}$ / μmol g$_{cat}^{-1}$ h^{-1}	r$_{CO}$ / μmol g$_{cat}^{-1}$ h^{-1}	S$_{MeOH}$ / %	S$_{DME}$ / %	S$_{CO}$ / %	X$_{CO2}$ / %
7000	27.1	20.9	761.3	3.3	5.0	91.7	2.6
10000	33.8	32.8	970.1	3.2	6.1	90.7	2.4
25000	41.6	42.3	926.5	4.0	8.0	88	0.7

3.2.3   Effect of Promoters on γ-Al$_2$O$_3$ Supported Catalysts

In this section, the difference of activity observed upon the loading of promoters with different percentages on γ-Al$_2$O$_3$ supported catalysts is reported and discussed.

3.2.3.1   Ga Effect

Four different Ga loadings on Cu/γ-Al$_2$O$_3$ catalyst are performed and the resulting catalysts' activity test results are shown in Table 3.11. It is observed that 5 wt. % Ga addition results in higher yield of DME and CO compared to Cu/γ-Al$_2$O$_3$, while methanol is almost similar in both catalysts. However, taking into account that DME is produced upon the dehydration of methanol, it is possible to say that 5 wt. % addition enhances the formation of methanol, as well as it facilitates its dehydration to DME. Higher Ga loadings (10 wt. %) showed less methanol and DME selectivity and yield compared to 5 wt. % loading. In addition, lower yield of CO is observed with higher Ga loading, with 12 wt. % being the lowest. According to XPS analysis by Medina et al.(34), Ga loading of 5 w. % resulted with higher dispersion than lower Ga loadings and unpromoted Cu/SiO$_2$, whilst Ga loading of 10 wt. % had a lower dispersion of Cu, which may explain the lower conversion of CO$_2$ on the higher Ga

loaded samples. It is worth noting that their TPR results did not show different Cu dispersion between different Ga loadings (2, 5 and 10 wt %), and they appeared to be lower in dispersion than unpromoted Cu/SiO_2. As reported previously in Table 3.2., it can be noted that the difference in XRD Cu crystal size is slight between 5 and 10 wt. % Ga promoted $Cu/\gamma-Al_2O_3$. Considering the XRD results obtained in this study, as well as the XPS and TPR results obtained by Medina et al.(32), it is difficult to attribute the high activity observed upon the addition of Ga to higher dispersion or smaller crystal size, but rather to its own interaction with Cu.

Table 3.11 Activity test results for Ga promoted $10Cu/\gamma-Al_2O_3$ with different Ga wt. % content, at 220 °C, 25,000 h^{-1} and $9H_2/1CO_2$

Catalyst	r_{MeOH} / μmol g_{cat}^{-1} h^{-1}	r_{DME} / μmol g_{cat}^{-1} h^{-1}	r_{CO} / μmol g_{cat}^{-1} h^{-1}	S_{MeOH} / %	S_{DME} / %	S_{CO} / %	X_{CO2} / %
$10Cu/\gamma-Al_2O_3$	49.4	44.0	477.5	8.0	14.3	77.7	0.4
$10Cu-5Ga/$ $\gamma-Al_2O_3$	52.5	96.5	957.1	4.4	16.1	79.5	0.8
$10Cu-10Ga/$ $\gamma-Al_2O_3$	41.6	42.3	926.5	4.0	8.0	88	0.7
$10Cu-12Ga/$ $\gamma-Al_2O_3$	50.6	34.1	692.8	6.2	8.4	85.4	0.5
$10Cu-15Ga/$ $\gamma-Al_2O_3$	50.1	41.8	787.8	5.5	9.1	85.4	0.6

3.2.3.2   Ho Effect

Ho is loaded with two different wt. % and the activity test results are shown in Table 3.12. It can be observed, that the addition of Ho decreases the selectivity of both methanol and DME, while it increases that of CO. In addition, methanol and CO

yield are observed to be the highest on 10 wt. % Ho, whilst DME is the lowest. The larger crystals formed on $10Cu-10Ho/\gamma-Al_2O_3$ shown in Table 3.2 may explain the higher yield of CO. For methanol, however, even though it has the highest yield on $10Cu-10Ho/\gamma-Al_2O_3$, DME yield being so low compared to $Cu/\gamma-Al_2O_3$ and $10Cu-2Ho/\gamma-Al_2O_3$ may be due to the basic sites on Ho_2O_3(76), which may have also enhanced CO_2 adsorption to increase its conversion.

Table 3.12 Activity test results for Ho promoted $10Cu/\gamma-Al_2O_3$ and $10Cu-5Ga/\gamma-Al_2O_3$ with different Ho wt. % content, at 220 °C, 25,000 h^{-1} and $9H_2/1CO_2$

Catalyst	r_{MeOH} / µmol $g_{cat}^{-1}h^{-1}$	r_{DME} / µmol $g_{cat}^{-1}h^{-1}$	r_{CO} / µmol $g_{cat}^{-1}h^{-1}$	S_{MeOH} / %	S_{DME} / %	S_{CO} / %	X_{CO2} / %
$10Cu/\gamma-Al_2O_3$	49.4	44.0	477.5	11.6	16.4	72.0	0.4
$10Cu-2Ho/\gamma-Al_2O_3$	27.2	26.6	746.0	3.3	6.4	90.3	1.8
$10Cu-10Ho/\gamma-Al_2O_3$	67.8	4.9	1253.0	5.1	0.7	94.2	0.8
$10Cu-5Ga/\gamma-Al_2O_3$	52.5	96.5	957.1	4.4	16.1	79.5	0.8
$10Cu-5Ga-5Ho/\gamma-Al_2O_3$	53.2	7.4	1213.5	4.2	1.1	94.7	1.2

3.2.3.3   La Effect

Loading of La is performed on $10Cu-5Ga/\gamma-Al_2O_3$ with 1 and 5 wt. %, and the resulting catalysts' activity test results are shown in Table 3.13. As can be observed, the catalyst activity is increased upon the addition of La, as CO_2 conversion is increased after La promotion. It is noted, however, that the increase in the activity is

more towards CO than it is towards methanol and DME, as the selectivity of CO is higher on La promoted catalysts. It is also observed that addition of La with high quantities (5 wt. %) results with a significant drop in the DME formation, as well as a decrease in methanol formation, while CO formation rate is almost doubled compared to 1 wt. %. It can be noted that the increase in the overall activity upon the addition of 1 wt. % of La may be attributed to the stronger CO_2 adsorption strength and capacity, as reported previously in literature(39). The decrease in DME formation at higher La loading (5 wt. %), however, may be due to the basicity of La_2O_3, as was observed for higher Ho loadings.

Table 3.13 Activity test results for La promoted 10Cu-5Ga/γ-Al_2O_3 with different La wt. % content, at 220 °C, 25,000 h^{-1} and 9H_2/1CO_2

Catalyst	r_{MeOH} / μmol $g_{cat}^{-1}h^{-1}$	r_{DME} / μmol $g_{cat}^{-1}h^{-1}$	r_{CO} / μmol $g_{cat}^{-1}h^{-1}$	S_{MeOH} / %	S_{DME} / %	S_{CO} / %	X_{CO2} / %
10Cu-5Ga/ γ-Al_2O_3	52.5	96.5	957.1	4.4	16.1	79.5	0.8
10Cu-5Ga- 1La/ γ-Al_2O_3	75.1	66.9	1817.2	3.7	6.6	89.7	1.3
10Cu-5Ga- 5La/ γ-Al_2O_3	59.7	3.8	3455.2	1.7	0.2	98.1	2.2

3.2.4 H^+-ZSM-5 Supported Catalysts

Some catalysts that are supported on H^+-ZSM5 have been tested and their results at 260 °C are shown in Table 3.14. As can be seen, and compared to γ-Al_2O_3 supported

catalysts, the overall activity of the catalysts is low, and the selectivity of both methanol and DME are low as well. In addition, methanol is further converted into ethane and propane, due to the high acidity of H^+-ZSM5(46). It can be noted that even though the temperature of the reaction is relatively high, CO is not formed with large quantities as found on γ-Al_2O_3 supported catalysts, which indicates fewer active Cu sites overall. Other results catalytic test results at 220 °C are reported in Table 3.15, indicating that lower temperatures do not help solving the problem of the activity of the H^+-ZSM5 supported catalysts. Due to the fact that metal loading is carried out via impregnation, it is possible that there are less available active sites due to possible ion-exchange that occurs between copper cations and the protons on H^+-ZSM5.Cu^{2+}-cations sites on zeolite would require higher temperatures to form metallic copper on the surface to react with CO_2. In addition, as was seen in Table 3.3, the external surface area is lower for H^+-ZSM5 supported catalysts, as opposed to other ones. This agrees also with the reported results in Table 3.2 regarding XRD crystal size and Fig. 3.5 regarding TEM images. The particle sizes found in the catalyst supported on H^+-ZSM5 have poor dispersion and larger particle and crystal sizes, which may explain the poor activity observed on H^+-ZSM5 supported catalysts. It is worth noting that, similar to the γ-Al_2O_3 supported catalysts case, Ho addition increased the activity of the catalyst, even though it was for CO not methanol, indicating possibly stronger adsorption of CO_2.

Table 3.14 Activity test results for H$^+$-ZSM5 supported catalysts at 260 °C.

Catalyst	r_{MeOH} / μmol $g_{cat}^{-1}h^{-1}$	r_{MeOH} / μmol $g_{cat}^{-1}h^{-1}$	$r_{Ethane+Propane}$ / μmol $g_{cat}^{-1}h^{-1}$	r_{CO} / μmol $g_{cat}^{-1}h^{-1}$	S_{MeOH} / %	S_{DME} / %	$S_{Ethane+Propane}$ / %	S_{CO} / %	X_{CO2} / %
10Cu-10Ga/H$^+$-ZSM5	7.1	8.3	13.2	460.9	1.4	3.2	6.7	88.7	0.4
10Cu-10Ho/H$^+$-ZSM5	6.4	2.0	5.4	1946.1	0.3	0.2	0.7	98.8	1.8
10Cu-5Ga-5Ho/ H$^+$-ZSM5	6.1	4.5	12.9	557.7	1.0	1.47	5.8	91.7	0.5

Table 3.15. Activity test results for 10Cu-10Ga/H$^+$-ZSM5 at 220 and 240 °C.

T / °C	r_{MeOH} / μmol $g_{cat}^{-1}h^{-1}$	r_{MeOH} / μmol $g_{cat}^{-1}h^{-1}$	r_C / μmol $g_{cat}^{-1}h^{-1}$	r_{CO} / μmol $g_{cat}^{-1}h^{-1}$	S_{MeOH} / %	S_{DME} / %	S_C / %	S_{CO} / %	X_{CO2} / %
220	0	5.8	5.8	120.4	0.0	8.3	5.8	85.9	0.1
240	4.8	8.7	17.9	251.0	1.7	6.0	6.1	86.2	0.6

3.2.5   CeO$_2$ Supported Catalysts

CeO$_2$ spheres that are synthesized following two different synthesis methods have been loaded with 10Cu-5Ga and catalytically tested. Results of the catalytic activity tests are shown in Table 3.16. As can be seen, the 2nd synthesis method resulted with higher activity towards the formation of methanol and CO, whilst selectivity is similar for both catalysts. As was observed previously, CeO$_2$ synthesized in the 2nd synthesis method has larger surface area than the 1st one, as shown in Table 3.3. In addition, Cu crystal sizes are found to be smaller on the 2nd one (higher surface area). The CeO$_2$ synthesized following the 2nd synthesis method was then loaded with La as well, and the results are shown in Table 3.13. It is observed that the addition of La with 1 wt. % has a negative effect on the catalyst activity. According to Table 3.2, the crystal size found on the catalyst after the addition of La is smaller than that for the unpromoted one, which may be due to better dispersion induced by La addition. However, it does not reflect on the results of the catalysts' activity.

Table 3.16 Activity test results for CeO_2 supported catalysts at 220 °C, 25,000 h^{-1} and $9H_2/1CO_2$

Catalyst	r_{MeOH} / μmol g_{cat}^{-1} h^{-1}	r_{DME} / μmol g_{cat}^{-1} h^{-1}	r_{CO} / μmol g_{cat}^{-1} h^{-1}	S_{MeOH} / %	S_{DME} / %	S_{CO} / %	X_{CO2} / %
10Cu-5Ga/ CeO$_2$ (1st)	12.4	0	468.7	2.6	0	97.4	0.3
10Cu/CeO$_2$ (2nd)	6.0	0	597.8	1.0	0	99.0	0.37
10Cu-5Ga/ CeO$_2$ (2nd)	49.4	0	2112.3	2.3	0	97.7	1.3
10Cu-5Ga-1La/ CeO$_2$ (2nd)	21.2	0	1104.5	1.9	0	98.1	0.7

3.2.6   SiO$_2$ Supported Catalysts

Activity tests are carried out on 10Cu-5Ga/SiO$_2$ and the results are shown in Table 3.17. As can be seen, using SiO$_2$ does not result with any improvement in terms of selectivity or activity of the catalyst. It was shown previously in Table 3.3 that possesses a large external surface area, whilst its crystal size is large compared to other catalysts, such as 10Cu-5Ga/γ-Al$_2$O$_3$. Taking into account both of the activity test results and characterization ones (XRD and BET and external surface areas), it can be noted that the use of supports that contribute to the reaction or interact well with the catalyst is necessary in order to achieve high activity and selectivity. Comparing SiO$_2$ supported catalyst results with that for H$^+$-ZSM5 supported one, it can be seen that a similar activity is observed, which is a weak one, where the interaction of the catalyst with the support is expected to be poor.

Table 3.17 Activity test results for 10Cu-5Ga/SiO$_2$ and 10Cu-5Ga/γ-Al$_2$O$_3$ at 220 °C, 25,000 h^{-1} and 9H$_2$/1CO$_2$

Catalyst	r_{MeOH} / μmol g$_{cat}^{-1}$ h^{-1}	r_{DME} / μmol g$_{cat}^{-1}$ h^{-1}	r_{CO} / μmol g$_{cat}^{-1}$ h^{-1}	S_{MeOH} / %	S_{DME} / %	S_{CO} / %	X_{CO2} / %
10Cu-5Ga/SiO$_2$	1.6	0.0	54	2.8	0	97.2	0.1
10Cu-5Ga/ γ-Al$_2$O$_3$	52.5	96.5	957.1	4.4	16.1	79.5	0.8

3.2.7   Comparison with the Commercial Catalyst

The results of some of the best performing catalysts in terms of high yield and selectivity of methanol and DME are reported again along with the commercial catalyst Cu/ZnO/Al$_2$O$_3$ and 10Cu-10Zn/γ-Al$_2$O$_3$ in Table 3.18 and Fig. 3.7. As can be seen, the addition of zinc results with a noticeable increase in methanol formation, as well as CO. Both catalysts, especially Cu/ZnO/Al$_2$O$_3$, however, have a high selectivity towards CO. Even though 10Cu-10Zn/γ-Al$_2$O$_3$ contains γ-Al$_2$O$_3$ as the support, which is acidic, the DME formation is nearly negligible compared to methanol and CO. This behavior may again be due to the fact that addition of ZnO increases the number of basic sites(77), which may interfere with the acidity of γ-Al$_2$O$_3$ with high Zn loading, similar to 10Cu-10Ho/γ-Al$_2$O$_3$ and 10Cu-5Ga-1La/γ-Al$_2$O$_3$. No DME was formed on Cu/ZnO/Al$_2$O$_3$ due to the fact that Al$_2$O$_3$ already exists in a trace fraction, acting as a structural promoter, unlike 10Cu-10Zn/γ-Al$_2$O$_3$, where γ-Al$_2$O$_3$ acts as a support. Based on the activity tests, it appears that the interaction between Ga$_2$O$_3$ and Cu resulted with better interaction than the SMSI between ZnO and Cu, as both of the Zn containing catalysts perform poorly in terms of methanol and DME selectivity.

The different effect of each promoter can be the result of the different interaction with Cu, which may be induced by the different atomic radii of those promoters(78). For example, it is possible that due to the large La atomic radius compared to other promoters used, only around 1% is required to enhance the activity, while further addition may block active sites on the catalyst, resulting with a reduction in activity towards methanol synthesis.

Table 3.18 Activity test results for the commercial catalyst against Ga and Ho promoted catalysts, at 220 °C, 25,000 h^{-1} and 9H$_2$/1CO$_2$

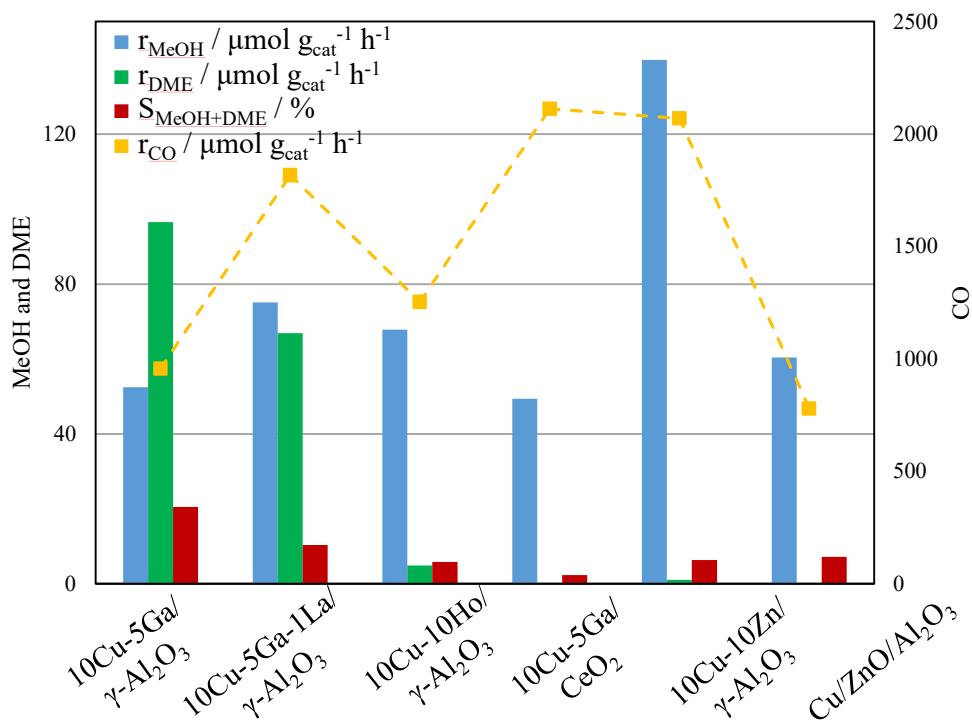| Catalyst	r_{MeOH} / µmol g_{cat}^{-1} h^{-1}	r_{DME} / µmol g_{cat}^{-1} h^{-1}	r_{CO} / µmol g_{cat}^{-1} h^{-1}	S_{MeOH} / %	S_{DME} / %	S_{CO} / %	X_{CO2} / %
10Cu-5Ga/ γ-Al$_2$O$_3$	52.5	96.5	957.1	4.4	16.1	79.5	0.8
10Cu-5Ga-1La/ γ-Al$_2$O$_3$	75.1	66.9	1817.2	3.7	6.6	89.7	1.3
10Cu-10Ho/ γ-Al$_2$O$_3$	67.8	4.9	1253.0	5.1	0.7	94.2	0.8
10Cu-5Ga/ CeO$_2$ (2nd)	49.4	0.0	2112.3	2.3	0	97.7	1.3
10Cu-10Zn/ γ-Al$_2$O$_3$	139.8	1.1	2069.3	6.3	0.1	93.6	1.3
Cu/ZnO/Al$_2$O$_3$	60.4	0.0	779.0	7.2	0	92.8	0.5

Figure 3.7 Activity test results for the commercial catalyst and Ga and Ho promoted catalysts, at 220 °C, 25,000 h^{-1} and 9H$_2$/1CO$_2$. The dashed yellow line for CO formation rate is a guide to the eye

Turnover frequency was also calculated for the same catalysts shown in Fig. 3.7., at 240 °C, and the results are reported in Table 3.19. As can be seen, the methanol TOF and combined methanol and DME TOF are found to be relatively high on the catalysts with larger particle sizes. The larger particles exhibiting the highest TOF can be attributed to the less available active sites (low dispersion) estimated which yet produce methanol with considerably large quantities, as in the case for 10Cu-10Zn/γ-Al$_2$O$_3$, in line with their low methanol activation energy values (Table 3.22).

Table 3.19 TOF of methanol and DME for different catalysts at 240 °C, 25,000 h^{-1} and 9H$_2$/1CO$_2$

Catalyst	d_c / nm	D / %	r_{MeOH} / µmol g_{cat}^{-1} h^{-1}	TOF_{MeOH} / s^{-1}	$TOF_{MeOH+DME}$ / s^{-1}
10Cu-5Ga/ γ-Al$_2$O$_3$	4	26	67.7	5.0×10^{-5}	1.3×10^{-4}
10Cu-5Ga- 1La/γ-Al$_2$O$_3$	13	8	92.1	2.2×10^{-4}	3.6×10^{-4}
10Cu-10Ho/ γ-Al$_2$O$_3$	50	2	81.8	7.7×10^{-4}	8.3×10^{-4}
10Cu-5Ga/ CeO$_2$ (2nd)	26	3	49.3	2.7×10^{-4}	2.7×10^{-4}
Cu/ZnO/Al$_2$O$_3$	26	8	82.8	4.4×10^{-4}	4.4×10^{-4}
10Cu-10Zn/ γ-Al$_2$O$_3$	40	4	147.2	1.0×10^{-3}	1.0×10^{-3}

3.2.8 Repeatability and Reproducibility

The repeatability of the results is ensured by carrying out the same catalytic test twice on the same catalyst from the same synthesized batch. This is performed over 10Cu-10Ga/γ-Al$_2$O$_3$ and 10Cu-10Ho/γ-Al$_2$O$_3$ and the results are reported in Table 3.20. As can be seen, the results are relatively similar to one another, and it is possible to say that they are repeatable.

Table 3.20 Repeated activity test results for 10Cu-10Ga/γ-Al$_2$O$_3$ and 10Cu-10Ho/γ-Al$_2$O$_3$ at 220 °C, 25,000 h^{-1} and 9H$_2$/1CO$_2$

Catalyst	Run	r_{MeOH} / μmol $g_{cat}^{-1}h^{-1}$	r_{DME} / μmol $g_{cat}^{-1}h^{-1}$	r_{CO} / μmol $g_{cat}^{-1}h^{-1}$	S_{MeOH} / %	S_{DME} / %	S_{CO} / %	X_{CO2} / %
10Cu-10Ga/	1	41.6	42.3	926.5	4.0	8.0	88	0.7
γ-Al$_2$O$_3$	2	33.2	35.6	842.0	3.5	7.5	89.0	0.6
10Cu-10Ho/	1	67.8	4.9	1253.0	5.1	0.7	94.2	0.8
γ-Al$_2$O$_3$	2	63.4	4.8	1176.7	5.1	0.8	94.1	0.8

In order to ensure reproducibility of the catalytic activity tests, 10Cu-10Ga/γ-Al$_2$O$_3$ catalyst is synthesized as two batches, each batch from scratch, and catalytic activity results are shown in Table 3.21. As can be seen, the results differ slightly from one another. Hence, the results can be said to be reproducible.

Table 3.21 Activity test results for the two batches of 10Cu-10Ga/γ-Al$_2$O$_3$ at 220 °C, 25,000 h^{-1} and 9H$_2$/1CO$_2$

Batch	r_{MeOH} / μmol g_{cat}^{-1} h^{-1}	r_{DME} / μmol g_{cat}^{-1} h^{-1}	r_{CO} / μmol g_{cat}^{-1} h^{-1}	S_{MeOH} / %	S_{DME} / %	S_{CO} / %	X_{CO2} / %
1st	39.8	25.3	929.4	3.9	5.0	91.1	2.3
2nd	33.8	32.8	970.1	3.2	6.1	90.7	2.4

3.2.9 Activation Energy

The activation energy of some of the catalysts are calculated and reported in Table 3.22. The activation energy of CO, as can be seen, is found to be always about 90-

100 kJ mol^{-1}, whilst it is the highest for the commercial catalyst Cu/ZnO/Al$_2$O$_3$. The activation energy of methanol appears to be the highest on CeO$_2$ supported catalysts. Based on the previous results of the catalytic activity tests at different temperatures in section 3.2.2.1, it is clear that the increase of temperature increases the formation rate of CO more than methanol and DME, as the selectivity of CO increases with temperature as shown in Table 3. The activation energy of methanol is decreased upon Zn and Ga addition to Cu catalysts. The lowest methanol activation energy is achieved on La promoted Cu-Ga/γ-Al$_2$O$_3$ catalyst (27 kJ mol^{-1}). Ga addition also decreases the DME formation activation energy, while Ho addition increases it. Activation energy of CO$_2$ is found to be close to CO, as CO is the major product in all of the catalysts.

Table 3.22 Activation energy results for different catalysts

Catalyst	$E_{a,MeOH}$ / kJ mol^{-1}	$E_{a,DME}$ / kJ mol^{-1}	$E_{a,CO}$ / kJ mol^{-1}	$E_{a,CO2}$ / kJ mol^{-1}
10Cu/γ-Al$_2$O$_3$	39	49	84	76
10Cu-5Ga/γ-Al$_2$O$_3$	32	32	92	80
10Cu-10Ga/γ-Al$_2$O$_3$	42	23	96	88
10Cu-12Ga/γ-Al$_2$O$_3$	35	41	91	84
10Cu-15Ga/γ-Al$_2$O$_3$	39	37	97	88
10Cu-10Ho/γ-Al$_2$O$_3$	36	64	97	93
10Cu-10Zn/γ-Al$_2$O$_3$	25	42	106	100
Cu/ZnO/Al$_2$O$_3$	32	-	116	104
10Cu-5Ga-La/γ-Al$_2$O$_3$	27	40	96	91
10Cu-5Ga/SiO$_2$	-	-	91	100
10Cu/CeO$_2$	77	-	88	88
10Cu-5Ga/CeO$_2$	34	-	109	106
10Cu-5Ga-La/CeO$_2$	45	-	93	92

CHAPTER 4

CONCLUSION

In this research, the hydrogenation of CO_2 to methanol and DME over promoted and supported Cu based catalysts has been investigated, by synthesizing Cu based catalysts with different promoters and supports, and testing their activity under different operating conditions. In addition, characterization techniques, including ICP-OES, XRD, N_2 adsorption/desorption, TEM and TPR were applied.

It was found that at temperatures of about 220 ℃, the catalysts exhibit the best activity and selectivity towards methanol and DME, while higher temperatures result with a higher CO formation. Those trends are, even though the reactions were operating far away from equilibrium, agree with thermodynamics. For space time velocity, reactions performed under its highest value (25,000 h^{-1}) showed the best activity and selectivity towards methanol and DME. Furthermore, the feed ratio of $9H_2/1CO_2$ turned out to be the optimal one.

The catalysts supported on γ-Al_2O_3 resulted with catalysts exhibiting higher activity and selectivity compared to H^+-ZSM5, SiO_2 and CeO_2 supported catalysts. Even though SiO_2 had a larger external surface area, it lacked the acidity as in the case of γ-Al_2O_3 and it did not disperse Cu well. H^+-ZSM5 had both smaller external surface area and low dispersion of Cu, as was observed in TEM and N_2 adsorption analysis. CeO_2, on the other hand, had the smallest surface area compared to all of the other three supports, yet it showed a better activity towards methanol and compared to SiO_2 and H^+-ZSM5, which may be attributed to the oxygen vacancies it creates. However, CeO_2 supported catalysts were not able to form DME due to the lack of acid sites.

Adding Ga as a promoter enhanced the activity and selectivity of the catalysts supported on γ-Al_2O_3 in terms of methanol and DME, and the selectivity of methanol

on CeO_2 supported one. Optimal Ga loading on γ-Al_2O_3 was found to be 5 wt.% for enhanced methanol and DME selectivity. Furthermore, addition of 1 wt.% La increased the overall activity of the Ga promoted γ-Al_2O_3 supported catalysts, while it decreased that for CeO_2 supported ones. On the other hand, addition of Ho resulted with a decrease in DME production, whilst an increase in methanol and CO yields was observed on γ-Al_2O_3 supported catalysts. The combined methanol and DME selectivity decreased upon Ho addition.

The higher selectivity towards the formation of methanol may attributed to smaller particles/crystals found on Cu-Ga/γ-Al_2O_3 catalysts. Higher particle sizes, on the other hand, may be responsible for the higher activity towards CO formation on γ-Al_2O_3 supported catalysts. For CeO_2 supported catalysts, it was observed that larger crystals observed on 10Cu-5Ga/CeO_2 compared to 10Cu/CeO_2 and 10Cu-5Ga-1La/CeO_2 resulted in better methanol activity and selectivity. Hence, as shown previously in the introduction, the increase in activity and selectivity of a catalyst may depend on the promoters and supports, and the intrinsic effect of particle size may not be present in our case, where different promoters and supports with different interaction with Cu are tested.

It was observed that the addition of Ho and La resulted in a significant decrease in DME formation, which may be due to their strong base sites, which did not allow methanol to dehydrate to DME, or due to their larger atomic radii compared to Ga. In addition, it was observed that the lowest combined selectivity of methanol and DME, or highest selectivity of CO, was observed on those catalysts that had a low activity towards DME formation. This point indicates the importance of involving methanol dehydration to DME reaction especially at the atmospheric pressure. From that perspective, catalysts producing high amounts of DME such as Cu-Ga/γ-Al_2O_3 catalysts would be preferred for higher combined methanol and DME selectivity.

CHAPTER 5

RECOMMENDATIONS

In this study, promising results in terms of activity towards methanol are found on Cu-Ga/CeO$_2$, which may be worth further investigation and optimization, whether with different CeO$_2$ synthesis methods or different metal loading techniques. In addition, in cases where DME production is low or negligible (i.e., CeO$_2$) better selectivity of methanol and DME may be achieved upon the use of dual pellets, where methanol synthesis catalysts and methanol dehydration to DME catalysts are pelleted separately and mixed. The use of dual beds of methanol synthesis catalyst followed by methanol dehydration to DME catalyst can help converting all methanol to DME, but it is unlikely to change the selectivity of methanol and DME. Instead, using triple beds or odd number of beds may achieve a higher selectivity as the complete (if possible) conversion of methanol to DME in each methanol dehydration bed, will allow further formation of methanol in the methanol synthesis bed. However, this configuration needs optimization as CO may end up increasing as well.

REFERENCES

1. Tans P (NOAA/GML), Keeling R (Scripps I of O. Trends in Atmospheric Carbon Dioxide [Internet]. Available from: gml.noaa.gov/ccgg/trends/

2. Damiani D, Litynski JT, Mcilvried HG, Vikara DM, Srivastava RD. The US Department of Energy's R&D program to reduce greenhouse gas emissions through benefi cial uses of carbon dioxide. Greenh Gas Sci Technol. 2012;2:9–19.

3. Rafiee A, Rajab Khalilpour K, Milani D, Panahi M. Trends in CO2 conversion and utilization: A review from process systems perspective. J Environ Chem Eng. 2018;6(5):5771–94.

4. Cecilia JA, Ballesteros Plata D, Vilarrasa García E. Co2 valorization and its subsequent valorization. Molecules. 2021;26(2):6–11.

5. Catizzone E, Bonura G, Migliori M, Frusteri F, Giordano G. CO2 recycling to dimethyl ether: State-of-the-art and perspectives. Molecules. 2018;23(1):1–28.

6. Ma Z, Porosoff MD. Development of Tandem Catalysts for CO2 Hydrogenation to Olefins. ACS Catal. 2019;9(3):2639–56.

7. Brady RN. Internal Combustion (Gasoline and Diesel) Engines. Reference Module in Earth Systems and Environmental Sciences. Elsevier Inc.; 2013. 1–59 p.

8. Kennedy GL. Dimethyl Ether. Encycl Toxicol Third Ed. 2014 Jan 1;160–1.

9. Din IU, Shaharun MS, Alotaibi MA, Alharthi AI, Naeem A. Recent developments on heterogeneous catalytic CO2 reduction to methanol. J CO2 Util. 2019;34(May):20–33.

10. Putrasari Y, Lim O. Dimethyl Ether as the Next Generation Fuel to Control Nitrogen Oxides and Particulate Matter Emissions from Internal Combustion Engines: A Review. ACS Omega. 2022;7(1):32–7.

11. Sheldon D. Methanol production - A technical history. Johnson Matthey Technol Rev. 2017;61(3):172–82.

12. Klier K. MethanoI Synthesis. Adv Catal. 1982;31:243–313.

13. Sahebdelfar S, Takht Ravanchi M. Carbon dioxide utilization for methane production: A thermodynamic analysis. J Pet Sci Eng. 2015;134:14–22.

14. Stangeland K, Kalai D, Li H, Yu Z. CO2 Methanation: The Effect of Catalysts and Reaction Conditions. Energy Procedia. 2017;105(1876):2022–7.

15. Lim Y, Lee CJ, Jeong YS, Song IH, Lee CJ, Han C. Optimal design and decision for combined steam reforming process with dry methane reforming to reuse CO 2 as a raw material. Ind Eng Chem Res. 2012;51(13):4982–9.

16. Torres Galvis HM, De Jong KP. Catalysts for production of lower olefins from synthesis gas: A review. ACS Catal. 2013;3(9):2130–49.

17. Ordomsky V V., Luo Y, Gu B, Carvalho A, Chernavskii PA, Cheng K, et al. Soldering of iron catalysts for direct synthesis of light olefins from syngas under mild reaction conditions. ACS Catal. 2017;7(10):6445–52.

18. Ojelade OA, Zaman SF. A review on CO2hydrogenation to lower olefins: Understanding the structure-property relationships in heterogeneous catalytic systems. J CO2 Util. 2021;47(March):101506.

19. Stangeland K, Li H, Yu Z. Thermodynamic Analysis of Chemical and Phase Equilibria in CO2 Hydrogenation to Methanol, Dimethyl Ether, and Higher Alcohols. Ind Eng Chem Res. 2018;57(11):4081–94.

20. Palomino RM, Ramírez PJ, Liu Z, Hamlyn R, Waluyo I, Mahapatra M, et al. Hydrogenation of CO2 on ZnO/Cu(100) and ZnO/Cu(111) Catalysts: Role of Copper Structure and Metal-Oxide Interface in Methanol Synthesis. J Phys Chem B. 2018;122(2):794–800.

21. Jiang X, Nie X, Guo X, Song C, Chen JG. Recent Advances in Carbon Dioxide Hydrogenation to Methanol via Heterogeneous Catalysis. Chem Rev. 2020;120(15):7984–8034.

22. Olah GA, Goeppert A, Prakash GKS. Chemical recycling of carbon dioxide to methanol and dimethyl ether: From greenhouse gas to renewable, environmentally carbon neutral fuels and synthetic hydrocarbons. J Org Chem. 2009;74(2):487–98.

23. Chinchen GC, Denny PJ, Jennings JR, Spencer MS, Waugh KC. Synthesis of Methanol. Part 1. Catalysts and Kinetics. ChemInform. 1988;19(22):1–65.

24. Arena F, Barbera K, Italiano G, Bonura G, Spadaro L, Frusteri F. Synthesis, characterization and activity pattern of Cu-ZnO/ZrO2 catalysts in the hydrogenation of carbon dioxide to methanol. J Catal. 2007;249(2):185–94.

25. Karelovic A, Ruiz P. The role of copper particle size in low pressure methanol synthesis via CO2 hydrogenation over Cu/ZnO catalysts. Catal Sci Technol. 2015;5(2):869–81.

26. Natesakhawat S, Lekse JW, Baltrus JP, Ohodnicki PR, Howard BH, Deng X, et al. Active sites and structure-activity relationships of copper-based catalysts for carbon dioxide hydrogenation to methanol. ACS Catal. 2012;2(8):1667–76.

27. Barberis L, Hakimioun AH, Plessow P, Visser NL, Stewart JA,

Vandegehuchte BD, et al. Competition between reverse water gas shift reaction and methanol synthesis from CO2: influence of copper particle size. Nanoscale. 2022.

28. Grunwaldt JD, Molenbroek AM, Topsøe NY, Topsøe H, Clausen BS. In Situ Investigations of Structural Changes in Cu/ZnO Catalysts. J Catal. 2000 10;194(2):452–60.

29. Behrens M, Studt F, Kasatkin I, Kühl S, Hävecker M, Abild-Pedersen F, et al. The active site of methanol synthesis over Cu/ZnO/Al2O 3 industrial catalysts. Science. 2012;336(6083):893–7.

30. Kang SH, Bae JW, Prasad PSS, Oh JH, Jun KW, Song SL, et al. Influence of Ga addition on the methanol synthesis activity of Cu/ZnO catalyst in the presence and absence of alumina. J Ind Eng Chem. 2009;15(5):665–9.

31. Ladera R, Pérez-Alonso FJ, González-Carballo JM, Ojeda M, Rojas S, Fierro JLG. Catalytic valorization of CO2 via methanol synthesis with Ga-promoted Cu-ZnO-ZrO2 catalysts. Appl Catal B Environ. 2013;142–143:241–8.

32. Medina JC, Figueroa M, Manrique R, Rodríguez Pereira J, Srinivasan PD, Bravo-Suárez JJ, et al. Catalytic consequences of Ga promotion on Cu for CO2 hydrogenation to methanol. Catal Sci Technol. 2017;7(15):3375–87.

33. Zohour B, Yilgor I, Gulgun MA, Birer O, Unal U, Leidholm C, et al. Discovery of Superior Cu-GaOx-HoOy Catalysts for the Reduction of Carbon Dioxide to Methanol at Atmospheric Pressure. ChemCatChem. 2016;8(8):1464–9.

34. Medina JC, Figueroa M, Manrique R, Rodríguez Pereira J, Srinivasan PD, Bravo-Suárez JJ, et al. Catalytic consequences of Ga promotion on Cu for CO2 hydrogenation to methanol. Catal Sci Technol. 2017;7(15):3375–87.

35. Hengne AM, Bhatte KD, Ould-Chikh S, Saih Y, Basset JM, Huang KW. Selective Production of Oxygenates from Carbon Dioxide Hydrogenation over a Mesoporous-Silica-Supported Copper-Gallium Nanocomposite Catalyst. ChemCatChem. 2018;10(6):1360–9.

36. Tezsevin I, Senkan S, Onal I, Düzenli D. DFT Study on the Hydrogenation of CO2 to Methanol on Ho-Doped Cu(211) Surface. J Phys Chem C. 2020;124(41):22426–34.

37. Guo X, Mao D, Lu G, Wang S, Wu G. The influence of la doping on the catalytic behavior of Cu/ZrO2 for methanol synthesis from CO2 hydrogenation. J Mol Catal A Chem. 2011;345(1–2):60–8.

38. Zuo J, Chen K, Zheng J, Ye L, Yuan Y. Enhanced CO2 hydrogenation to methanol over La oxide-modified Cu nanoparticles socketed on Cu phyllosilicate nanotubes. J CO2 Util. 2021;52(August):101699.

39. Chou CY, Lobo RF. Direct conversion of CO2 into methanol over promoted indium oxide-based catalysts. Appl Catal A Gen. 2019;583(July):117144.

40. Chen K, Fang H, Wu S, Liu X, Zheng J, Zhou S, et al. CO2 hydrogenation to methanol over Cu catalysts supported on La-modified SBA-15: The crucial role of Cu–LaOx interfaces. Appl Catal B Environ. 2019;251(March):119–29.

41. Gafurov MR, Mukhambetov IN, Yavkin B V., Mamin G V., Lamberov AA, Orlinskii SB. Quantitative Analysis of Lewis Acid Centers of γ-Alumina by Using EPR of the Adsorbed Anthraquinone as a Probe Molecule: Comparison with the Pyridine, Carbon Monoxide IR, and TPD of Ammonia. J Phys Chem C. 2015;119(49):27410–5.

42. Palčić A, Valtchev V. Analysis and control of acid sites in zeolites. Appl Catal A Gen. 2020;606(May 2020):117795.

43. Busca G. Acidity and basicity of zeolites: A fundamental approach. Microporous Mesoporous Mater. 2017;254(June 2016):3–16.

44. Phung TK, Busca G. On the Lewis acidity of protonic zeolites. Appl Catal A Gen. 2015;504:151–7.

45. Frusteri F, Bonura G, Cannilla C, Ferrante GD, Aloise A, Catizzone E, et al. Applied Catalysis B : Environmental Stepwise tuning of metal-oxide and acid sites of CuZnZr-MFI hybrid catalysts for the direct DME synthesis by CO2 hydrogenation. Applied Catal B, Environ. 2015;176–177:522–31.

46. Catizzone E, Aloise A, Migliori M, Giordano G. From 1-D to 3-D zeolite structures: performance assessment in catalysis of vapour-phase methanol dehydration to DME. Microporous Mesoporous Mater. 2017;243:102–11.

47. Hassanpour S, Taghizadeh M. Preparation , Characterization , and Activity Evaluation of H-ZSM-5 Catalysts in Vapor-Phase Methanol Dehydration to Dimethyl Ether. 2010;4063–9.

48. TROVARELLI A. Catalytic Properties of Ceria and Ce02-Containing Materials. Catal Rev Sci Eng. 1996;38:439–520.

49. Yang SC, Su WN, Rick J, Lin SD, Liu JY, Pan CJ, et al. Oxygen vacancy engineering of cerium oxides for carbon dioxide capture and reduction. ChemSusChem. 2013;6(8):1326–9.

50. Wang W, Qu Z, Song L, Fu Q. CO2 hydrogenation to methanol over Cu/CeO2 and Cu/ZrO2 catalysts: Tuning methanol selectivity via metal-support interaction. J Energy Chem. 2020;40:22–30.

51. Tan Q, Shi Z, Wu D. CO2 hydrogenation over differently morphological CeO2-supported Cu-Ni catalysts. Int J Energy Res. 2019;43(10):5392–404.

52. Studt F, Sharafutdinov I, Abild-Pedersen F, Elkjær CF, Hummelshøj JS, Dahl

S, et al. Discovery of a Ni-Ga catalyst for carbon dioxide reduction to methanol. Nat Chem. 2014;6(4):320–4.

53. García-Trenco A, Regoutz A, White ER, Payne DJ, Shaffer MSP, Williams CK. PdIn intermetallic nanoparticles for the Hydrogenation of CO2 to Methanol. Appl Catal B Environ. 2018;220:9–18.

54. Jiang X, Jiao Y, Moran C, Nie X, Gong Y, Guo X, et al. CO2 hydrogenation to methanol on Pd–Cu bimetallic catalysts with lower metal loadings. Catal Commun. 2019;118(May 2018):10–4.

55. Ye J, Liu C, Mei D, Ge Q. Active Oxygen Vacancy Site for Methanol Synthesis from CO 2 Hydrogenation on In2O3 (110): A DFT Study. 2013;3(110).

56. Sun K, Fan Z, Ye J, Yan J, Ge Q, Li Y, et al. Hydrogenation of CO2 to methanol over In2O3 catalyst. J CO2 Util. 2015;12:1–6.

57. Bansode A, Urakawa A. Towards full one-pass conversion of carbon dioxide to methanol and methanol-derived products. J Catal. 2014;309:66–70.

58. Ruland H, Song H, Laudenschleger D, Stürmer S, Schmidt S, He J, et al. CO2 Hydrogenation with Cu/ZnO/Al2O3: A Benchmark Study. ChemCatChem. 2020;12(12):3216–22.

59. Díez-Ramírez J, Dorado F, De La Osa AR, Valverde JL, Sánchez P. Hydrogenation of CO2 to Methanol at Atmospheric Pressure over Cu/ZnO Catalysts: Influence of the Calcination, Reduction, and Metal Loading. Ind Eng Chem Res. 2017;56(8):1979–87.

60. Cai W, De La Piscina PR, Toyir J, Homs N. CO2 hydrogenation to methanol over CuZnGa catalysts prepared using microwave-assisted methods. Catal Today. 2015;242(Part A):193–9.

61. Allam D, Bennici S, Limousy L, Hocine S. Improved Cu- and Zn-based catalysts for CO2 hydrogenation to methanol. Comptes Rendus Chim. 2019;22(2–3):227–37.

62. Jiang X, Koizumi N, Guo X, Song C. Bimetallic Pd-Cu catalysts for selective CO2 hydrogenation to methanol. Appl Catal B Environ. 2015;170–171:173–85.

63. Bahruji H, Armstrong RD, Ruiz Esquius J, Jones W, Bowker M, Hutchings GJ. Hydrogenation of CO2 to Dimethyl Ether over Brønsted Acidic PdZn Catalysts. Ind Eng Chem Res. 2018;57(20):6821–9.

64. Choi EJ, Lee YH, Lee DW, Moon DJ, Lee KY. Hydrogenation of CO2 to methanol over Pd–Cu/CeO2 catalysts. Mol Catal. 2017;434(2017):146–53.

65. Tan Q, Shi Z, Wu D. CO2 Hydrogenation to Methanol over a Highly Active Cu-Ni/CeO2-Nanotube Catalyst. Ind Eng Chem Res. 2018;57(31):10148–58.

66. Hu ZM, Takahashi K, Nakatsuji H. Mechanism of the hydrogenation of CO2 to methanol on a Cu(100) surface: dipped adcluster model study. Surf Sci. 1999;442(1):90–106.

67. Malik AS, Zaman SF, Al-Zahrani AA, Daous MA, Driss H, Petrov LA. Development of highly selective PdZn/CeO2 and Ca-doped PdZn/CeO2 catalysts for methanol synthesis from CO2 hydrogenation. Appl Catal A Gen. 2018;560(February):42–53.

68. Kattel S, Yan B, Yang Y, Chen JG, Liu P. Optimizing Binding Energies of Key Intermediates for CO2 Hydrogenation to Methanol over Oxide-Supported Copper. J Am Chem Soc. 2016;138(38):12440–50.

69. Mei C, Wen P, Liu Z, Liu H, Wang Y, Yang W, et al. Selective production of propylene from methanol: Mesoporosity development in high silica HZSM-5. J Catal. 2008;258(1):243–9.

70. Sun C, Sun J, Xiao G, Zhang H, Qiu X, Li H, et al. Mesoscale organization of nearly monodisperse flowerlike ceria microspheres. J Phys Chem B. 2006;110(27):13445–52.

71. Baltes C, Vukojević S, Schüth F. Correlations between synthesis, precursor, and catalyst structure and activity of a large set of CuO/ZnO/Al2O3 catalysts for methanol synthesis. J Catal. 2008;258(2):334–44.

72. Munnik P, De Jongh PE, De Jong KP. Recent Developments in the Synthesis of Supported Catalysts. Chem Rev. 2015;115(14):6687–718.

73. Ahmad K, Upadhyayula S. Greenhouse gas CO2 hydrogenation to fuels: A thermodynamic analysis. Environ Prog Sustain Energy. 2019;38(1):98–111.

74. Lee JS, Han SH, Kim HG, Lee KH, Kim YG. Effects of Space Velocity on Methanol Synthesis from CC2/CO/H2 over Cu/ZnO/Al2O3 Catalyst. Korean J Chem Eng. 2000;17(3):332–6.

75. Martin O, Martín AJ, Mondelli C, Mitchell S, Segawa TF, Hauert R, et al. Indium oxide as a superior catalyst for methanol synthesis by CO2 hydrogenation. Angew Chemie - Int Ed. 2016;55(21):6261–5.

76. Mekhemer GAH. Surface acid-base properties of holmium oxide catalyst: In situ infrared spectroscopy. Appl Catal A Gen. 2004;275(1–2):1–7.

77. Jiang F, Yang Y, Wang L, Li Y, Fang Z, Xu Y, et al. Dependence of copper particle size and interface on methanol and CO formation in CO2 hydrogenation over Cu@ZnO catalysts. Catal Sci Technol. 2022;12(2):551–64.

78. Özbek MO, Önal I, vanSanten RA. Chlorine and Caesium Promotion of Silver Ethylene Epoxidation Catalysts. ChemCatChem. 2013;5(2):443–51.

APPENDICES
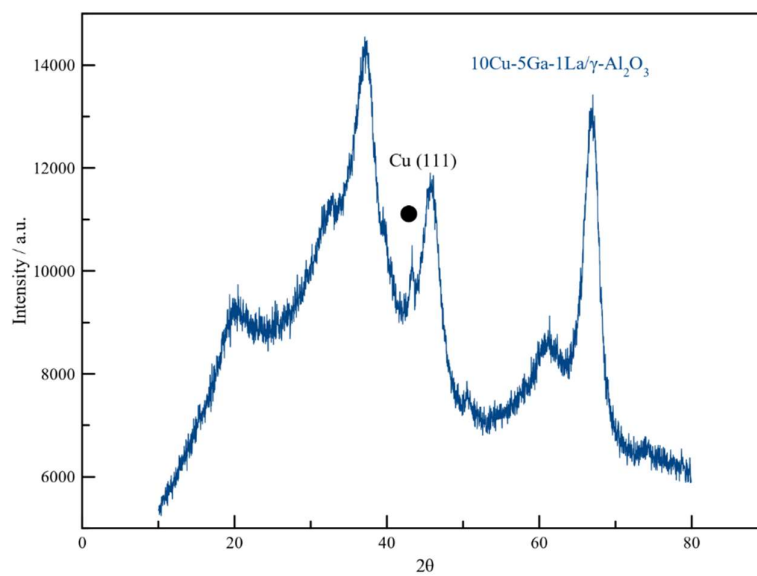
A. XRD Pattern of Some Catalysts

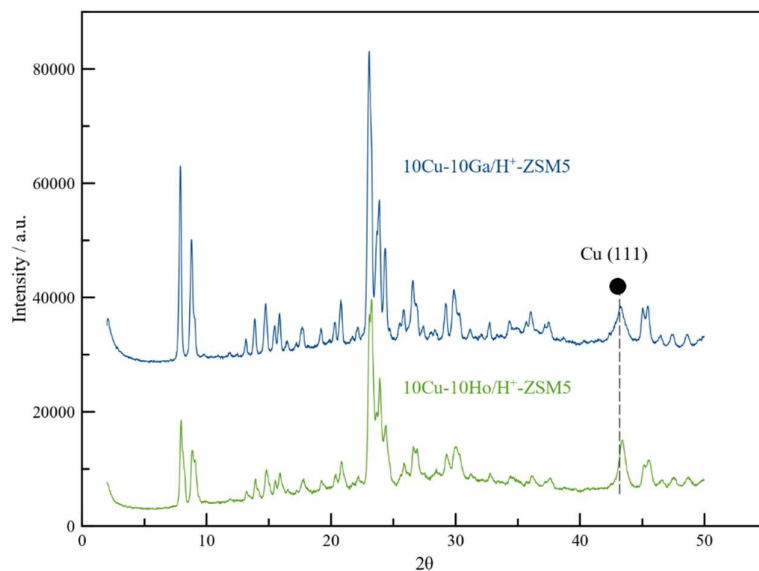Figure A.1 XRD pattern of 10Cu-Ga-1La/γ-Al$_2$O$_3$ (λ=1.5418 Å)

Figure A.2 XRD pattern of 10Cu-10Ga/H$^+$-ZSM5 and 10Cu-10Ho/H$^+$-ZSM5
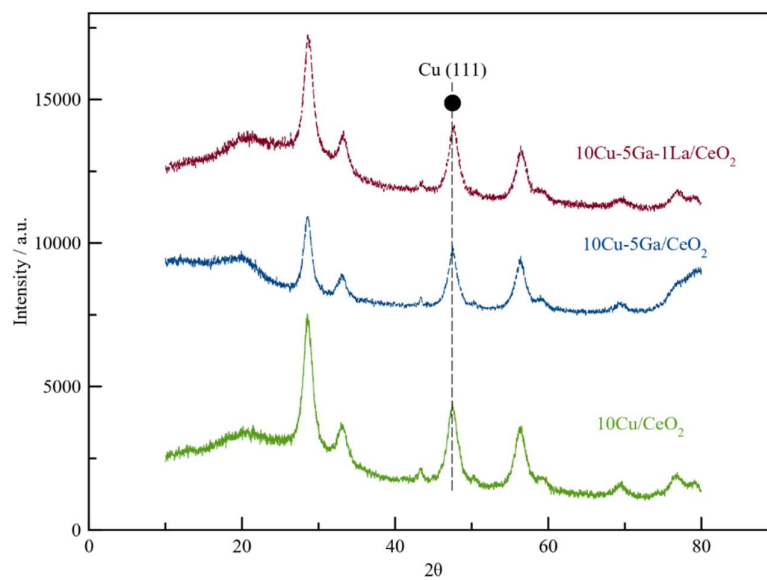(λ=1.5418 Å)

Figure A.3 XRD pattern of 10Cu/CeO$_2$, 10Cu-5Ga/CeO$_2$ and 10Cu-5Ga-1La/CeO$_2$
(λ=1.5418 Å)

B. TEM-EDX Mapping of Some Catalysts

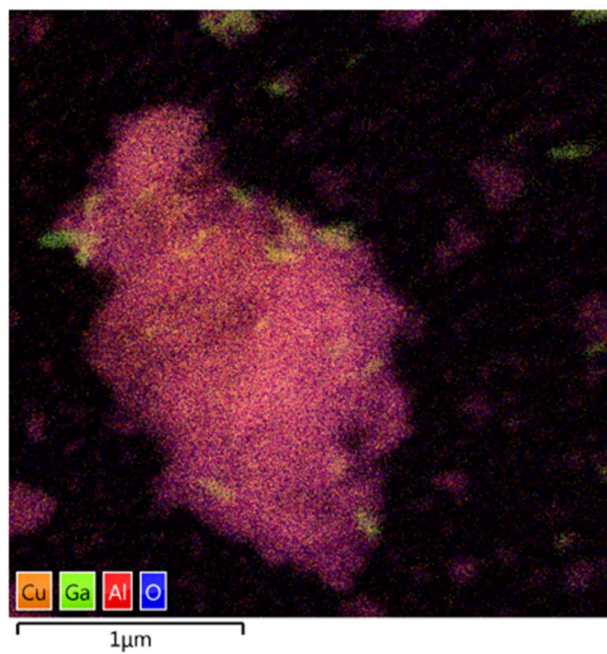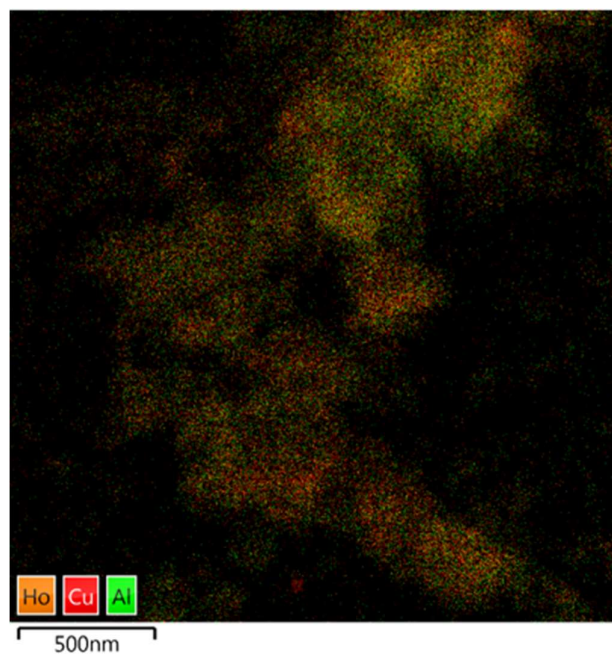

Figure B.1 TEM-EDX mapping of 10Cu-10Ga/γ-Al$_2$O$_3$
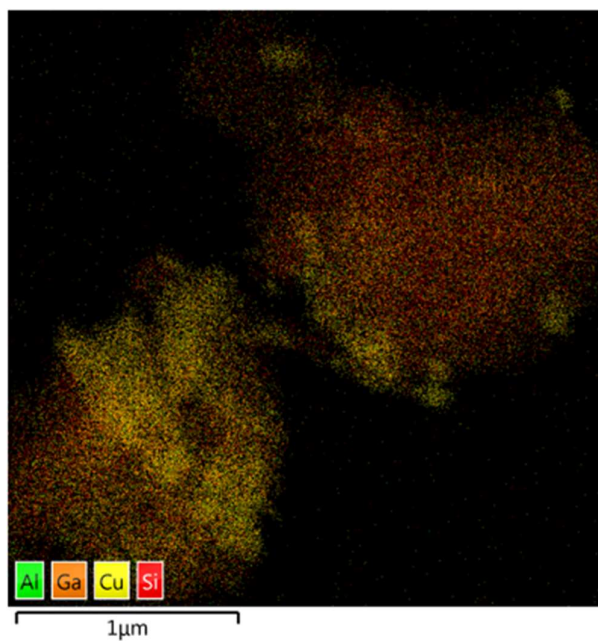

Figure B.2 TEM-EDX mapping of 10Cu-10Ho/γ-Al$_2$O$_3$

Figure B.3 TEM-EDX mapping of 10Cu-10Ga/H$^+$-ZSM-5
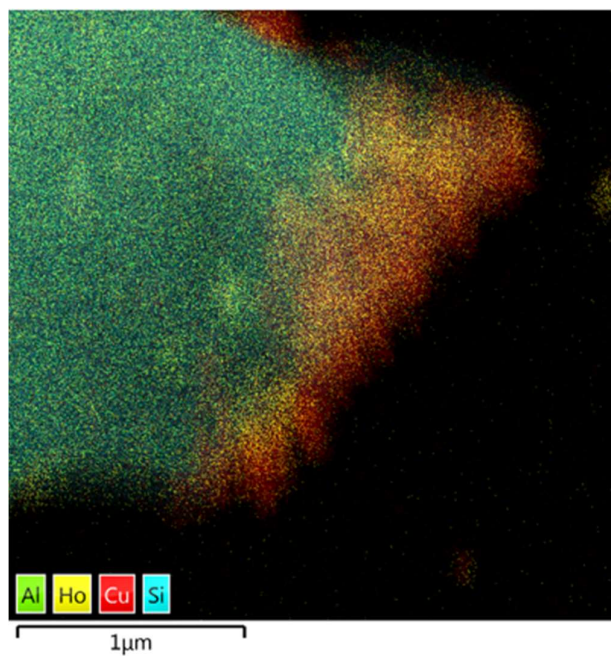
Figure B.4 TEM-EDX mapping of 10Cu-10Ho/H$^+$-ZSM-5

C. Sample Calculation on Activity Test Results of $10Cu-10Ga/\gamma-Al_2O_3$

In this section, a few sample calculations will be made to demonstrate how the activity test results were obtained.

C1. Formation Rates

Methanol, DME and CO formation rates are calculated using Eq. 2.9:

$$r_{MeOH} = \frac{v_{total} P f_r A}{RT} \quad _{cat}$$

where;

v_{total} = 112 cm^3 min^{-1}

P = 101325 Pa

T = 23 °C

m_{cat} = 200 mg

R = 8.314 Pa m^3 mol^{-1} K^{-1}

For methanol:

$f_{r_{MeOH}}$ = 0.665 ppm area^{-1}

A_{MeOH} = 45.3 area

Hence,

$$r_{MeOH} = \frac{112\frac{cm^3}{min} \times 101325\ Pa \times 0.665\frac{ppm}{area} \times 45.3\ area}{8.314\frac{Pa\ m^3}{mol\ K} \times (23+27\ .15)\ K \times 200\ mg_{cat}} \times \frac{10^3\ mg_{cat}}{1\ g_{cat}} \times \frac{1\ m^3}{10^6\ cm^3} \times \frac{10^6\ \mu mol}{1\ mol} \times$$

$$\frac{1}{10^6\ ppm} \times \frac{60\ min}{1\ h}$$

$$r_{MeOH} = 41.6\ \frac{\mu mol}{g_{cat}\ h}$$

For DME:

$f_{r_{DME}}= 0.425$ ppm area^{-1}

$A_{DME}= 71.7$ area

Hence,

$$r_{DME} = \frac{112\frac{cm^3}{min}\times101325\ Pa\times0.425\frac{ppm}{area}\times71.7\ area}{8.314\frac{Pa\ m^3}{mol\ K}\times(23+27\ .15)\ K\times200\ mg_{cat}} \times \frac{10^3\ mg_{cat}}{1\ g_{cat}} \times \frac{1\ m^3}{10^6\ cm^3} \times \frac{10^6\ \mu mol}{1\ mol} \times$$

$$\frac{1}{10^6 ppm} \times \frac{60\ min}{1\ h}$$

$$r_{DME} = 42.3\ \frac{\mu mol}{g_{cat}\ h}$$

For CO:

$f_{r_{CO}}= 1.249$ ppm area^{-1}

$A_{CO}= 475.4$ area

Hence,

$$r_{CO} = \frac{112\frac{cm^3}{min}\times101325\ Pa\times1.249\frac{ppm}{area}\times475.4\ area}{8.314\frac{Pa\ m^3}{mol\ K}\times(23+273.15)\ K\times200\ mg_{cat}} \times \frac{10^3\ mg_{cat}}{1\ g_{cat}} \times \frac{1\ m^3}{10^6\ cm^3} \times \frac{10^6\ \mu mol}{1\ mol} \times$$

$$\frac{1}{10^6 ppm} \times \frac{60\ min}{1\ h}$$

$$r_{CO} = 926.5\ \frac{\mu mol}{g_{cat}\ h}$$

C2. Products Selectivity

Selectivity is found using Eq. 2.7:

$$S_i = \frac{c_i\ r_i}{\sum_i c_i r_i}$$

For methanol:

$$S_{MeOH} = \frac{1\times41.6}{1\times41.6+2\times42.3+1\times926.5}$$

$$S_{MeOH} = 4.0\ \%$$

For DME:

$$S_{DME} = \frac{2 \times 42.3}{1 \times 41.6 + 2 \times 42.3 + 1 \times 926.5} \times 100\%$$

$$S_{DME} = 8.0\%$$

For CO:

$$S_{CO} = \frac{1 \times 926.5}{1 \times 41.6 + 2 \times 42.3 + 1 \times 926.5} \times 100\%$$

$$S_{CO} = 88.0\%$$

C3. CO_2 Conversion

CO_2 conversion is calculated using Eq. 2.8:

$$X_{CO_2} = \frac{\sum_i c_i r_i}{F_{CO_{2_{inlet}}}/m_{cat}}$$

where $F_{CO_{2_{inlet}}} = 22630 \frac{\mu mol}{h}$

Hence,

$$X_{CO_2} = \frac{1 \times 41.6 + 2 \times 42.3 + 1 \times 926.5}{\frac{22630}{0.2}} \times 100\%$$

$$X_{CO_2} = 1.0\%$$